
(Unterschrift Betreuer)



TECHNISCHE
UNIVERSITÄT
WIEN

Vienna University of Technology

DIPLOMARBEIT

Investigation of a dual-colour magneto-optical trap

Ausgeführt am Atominstitut
der Technischen Universität Wien

Unter der Anleitung von
Univ.Prof. Thorsten Schumm und Professor Peter Krüger

durch
Robert Hollenstein

Gumpendorfer Strasse 135/32 1060 Wien

11.2.2014

Untersuchungen an einer bichromatischen magneto-optischen Falle

Die magneto-optische-Falle (MOT) ist ein Grundbaustein bei fast allen Experimenten mit ultrakalten Atomen. Mit ihr können neutrale Atome gefangen und auf Temperaturen unter 1 mK gekühlt werden. Eine verbesserte Performance der MOT bezüglich Laderate und erreichbarer Atomzahl ist von grossem Nutzen für Experimente. Das Ziel unseres Experiments ist es ultrakalte Atome als Sensoren einzusetzen. Hierfür ist es notwendig ein sehr gutes Vakuum aufrecht zu halten und einen flexiblen Aufbau zu haben. In dieser Arbeit wird eine neuartige Variante der MOT - eine bichromatische MOT - vorgestellt und untersucht. Es wird gezeigt, dass durch die Verwendung von zwei Laserfrequenzen bei gleichbleibender Laserleistung die Performance der MOT deutlich verbessert werden kann. Dadurch bleibt ein sehr gutes Vakuum für das Experiment erhalten. Für die geplanten Experimente mit ultrakalten Atomen als Sensoren wurde eine Halterung mit Vakuumdurchführungen entworfen. Diese Halterung garantiert die Flexibilität des Aufbaus für zukünftige Experimente.

Investigation of a dual-colour magneto-optical trap

The magneto-optical trap (MOT) is a basic prerequisite of almost all experiments with ultra-cold atoms. It captures and traps neutral atoms and cools them to temperatures below 1 mK. An enhanced performance of a MOT regarding loading rate and achievable atom number is of great value for experiments. The goal of our experiment is using ultra-cold atoms as sensors. Therefore it is essential to maintain a very good vacuum and to have a flexible set-up. In this work a novel variant of a MOT - a dual-colour MOT - is presented and investigated. It is shown, that through the use of two laser frequencies the performance of the MOT can be increased significantly while keeping the same laser power. Therefore a very good vacuum can be maintained. For the planned experiments with ultra-cold atoms a mounting with vacuum feedthroughs has been designed. This mounting guarantees the flexibility of the set-up for future experiments.

Contents

1. Introduction	6
2. Theory of magneto-optical trapping	8
2.1. Light force on an atom	8
2.2. Trapping in momentum space	9
2.3. Doppler limit	10
2.4. Trapping in real space	10
2.5. Six-beam MOT	11
2.6. Polarisation gradient cooling	12
2.7. Rubidium	13
2.8. Repumping	13
2.9. MOT dynamics	14
2.10. Temperature of a cloud of atoms	14
3. Experiment	17
3.1. The MOT in our experiment	17
3.1.1. Reflection MOT	17
3.1.2. Dual-colour MOT	18
3.2. Set-up	18
3.2.1. Vacuum chamber	18
3.2.2. Quadrupole Coils	21
3.2.3. Laser set-up	22
3.2.4. Imaging system	23
4. Dual-colour MOT	25
4.1. Introduction	25
4.2. Measurements	26
4.2.1. Overview	26
4.2.2. Calibration and test measurements	26
4.2.3. First dual-colour MOTs	28
4.2.4. Getting the MOT in shape	29
4.2.5. Scanning the frequency domain	30
4.2.6. Loading	30
4.2.7. Power ratios	33
4.2.8. Temperature	33
4.2.9. Power	35
4.3. Conclusion	35
5. Towards ultra-close trapping	37
5.1. Introduction	37
5.2. Five-beam MOT	38

5.3. Magnetic fields	39
5.3.1. Magnetic trapping structures	39
5.3.2. MOT coils	40
5.4. Mounting	42
5.4.1. Prerequisites for the mounting	42
5.4.2. Design	42
5.4.3. Temperature simulations	46
6. Conclusion and outlook	49
A. Technical drawings	51
Bibliography	56
Danksagung	59

1. Introduction

Cold atom experiments have received a big boost in the last years. Although theories for cooling and trapping atoms with light are over 50 years old, the first experiments to succeed in this task were towards the end of the 80's. For this achievement - the development of methods to cool and trap atoms with laser light - the Nobel price for physics was awarded in 1997 to Steven Chu [1], Claude Cohen-Tannoudji [2] and William D. Phillips [3]. In a magneto-optical trap (MOT) a dilute cloud of neutral atoms is gathered and cooled to temperatures below 1 mK. This cloud of cold atoms can be used for a lot of different interesting experiments. One of the most interesting achievable phenomena is the Bose-Einstein condensation (BEC). The cold cloud is transferred into a magnetic trap or optical dipole trap and further cooled by evaporative cooling to nK where a phase transition to the quantum mechanical BEC phase occurs. This has been achieved in 1995 [4] [5] [6]. Only six years later Eric A. Cornell, Carl E. Wiemann [7] and Wolfgang Ketterle [8] received the Nobel price in physics for the achievement of Bose-Einstein condensation.

Many interesting phenomena can be observed with cold atoms and they can be used for quantum simulation or quantum computing, e.g. : Wildermuth et al. used a BEC to image the current density inside a conductor by probing the generated magnetic field [9] [10]. Bloch et al. used cold atoms as quantum simulators [11]. Investigations of the Bose-Hubbard model and superfluid-to-Mott insulator transition have been conducted by Bakr et al. with cold atoms [12]. Electromagnetically induced transparency has been used by Hau et al. [13] to slow light by many orders of magnitude and by Liu et al. [14] to even stop light and to store coherent information of the light in the cloud of cold atoms. Chanelière et al. managed to transfer quantum information between two quantum memories of cold atoms [15]. Rauschenbeutel et al. trapped atoms close to nanofibres, where the atoms are efficiently interfaced with resonant light through the nanofibre [16].

The MOT is in itself already a powerful source of cold atoms and a lot of groups strive to increase its performance through different means. William D. Phillips used a Zeeman slower¹ to get the atoms to slower velocities before capturing them in a MOT [3]. A different set-up to pre-cool atoms for MOT loading is a 2D MOT² [17]. Another approach to increase the performance of a MOT is the dark MOT³ [18]. It does not increase the loading rate like the previous mentioned set-ups but decreases

¹Zeeman slower: A magnetic field gradient along the path between the source of atoms (oven) and the MOT in which the atoms are slowed by a counter propagating laser. Velocity-dependent Doppler shift and Zeeman splitting cancel each other along the path in a way that the atoms are slowed along the whole path from a few 100 m/s to about 10 m/s.

²2D MOT: A source beam is slowed in the radial direction by four laser beams. Only sufficiently slowed atoms are able to pass an aperture to the final MOT.

³Dark MOT or dark SPOT: the centre of the MOT is not illuminated by the repumping laser. The atoms in the middle of the MOT fall to a dark state and don't contribute to light induced collisions which limit the density of the MOT.

the loss rate in the MOT.

The research interests of our group are atom-surface interactions, precise sensing and trapping below one micron from the surface (ultra-close trapping). For all experiments in these fields it is mandatory to have a very low background pressure in the vacuum system. First, because of contamination of the samples or surfaces and second, because of long lifetimes of the trapped ultra-cold atoms [19]. In single chamber systems one has to make a trade-off between higher background pressure, hence better performance of the MOT or lower background pressure, therefore a long lifetime of the trapped atoms.

The dual-colour MOT presented in this thesis, so called as two different laser frequencies are used as cooling beams, has an improved performance compared to single-colour MOTs and therefore allows an operation at lower background pressure. Albeit its advantages, not many groups have investigated dual-colour MOTs. The most noteworthy papers on dual-colour MOTs are from Sinclair, Riis and Snadden [20] and Cao, Luo, Wang, Chen and Wang [21].

The goal of this thesis was to achieve a better performance in a MOT with some restrictions which stem from the planned experiments in the chamber and the experimental set-up. The approach described here is a dual-colour MOT. A dual-colour MOT uses the same set-up as a normal MOT but uses two laser frequencies for cooling on the cooling transition. The two laser frequencies are quite close (relative detuning of about half the natural line width of the cooling transition). It is shown that with this technique the loss rate can be significantly reduced and therefore the number of atoms increased while also keeping the same temperature of the atomic cloud. Furthermore this dual-colour MOT would be quite easy to implement on other existing experiments where a single-colour MOT is present. Depending on the specific set-up it would be possible to add the second frequency by just adapting the electronics for the acousto-optical modulator that controls the cooling frequency. No adjustment on the laser table or the experimental set-up would be needed.

Another goal was to further advance the whole experiment which will bring cold atoms close to thin surfaces. Because our future samples are not reflective a normal 45° mirror MOT is not possible and a new approach – a five-beam MOT⁴ – is designed.

The structure of this thesis is as follows. The next chapter introduces theoretical foundations for magneto-optical trapping with respect to the particular specialities of this thesis. Chapter 3 describes the experimental set-up used for this thesis. Chapter 4 goes deeper into the investigation of the dual-colour MOT with the experimental results. Chapter 5 describes technology that leads to ultra close trapping of cold atoms near surfaces and also includes the design of the mounting for future experiments on this topic. The last chapter contains the conclusion and an outlook.

⁴Five-beam MOT: Special case of a six-beam MOT. The four horizontal laser beams are kept as is. The beam from the bottom is reflected on the surface of the mounting through a $\lambda/4$ -plate to produce the sixth beam with the correct polarisation.

2. Theory of magneto-optical trapping

This chapter is about the workings of magneto-optical trapping and how we implemented it into our setup. A magneto-optical trap (MOT) uses a combination of magnetic fields and lasers to capture neutral atoms and cool them to temperatures below 1 mK. An in-depth explanation and further theory can be found in the book of Metcalf and Van der Straten [22]. We will refrain from giving a detailed theoretical explanation and will only explain the basic principles of a MOT.

In a typical MOT six laser beams (three counter-propagating pairs) with specific polarisations overlap in the zero-point of a magnetic quadrupole field. This zero-point resides in a vacuum chamber where some of the atoms of the isotope that is being trapped are present. In our case these atoms are Rubidium 87 (^{87}Rb). The explanations given here use simplified models in one dimension but can be extended to three dimensions.

2.1. Light force on an atom

We will describe an atom as a two-level system that is coupled to a monochromatic light field. Even though in reality atoms have more than two energy levels, this description is appropriate because a laser is a very narrow-band light source and almost¹ only addresses two levels of the atoms.

Using the dipole approximation² and rotating wave approximation³ we can derive an expression for the force of a laser with intensity I acting on an atom with velocity \vec{v}

$$\vec{F} = \hbar \vec{k} \frac{\Gamma}{2} \frac{\frac{I}{I_0}}{1 + \frac{I}{I_0} + \left[\frac{2(\delta - \vec{k} \cdot \vec{v})}{\Gamma} \right]^2}, \quad (2.1)$$

where \vec{k} is the wave vector of the laser light, Γ is the natural linewidth of the atomic transition and $\delta = \omega_L - \omega_0$ is the detuning between laser light and atomic transition,

¹In case more than one level is addressed and therefore the atom could be lost from the cooling cycle, an additional laser frequency is used to “pump” the atom back into one of the intended states, see section 2.8 for more details.

²Dipole approximation: the wavelength λ of the light is much larger than the size of the atom. Therefore the atom can be described as a point-like dipole with energy $E_{\text{dipole}} = -\vec{d} \cdot \vec{E}(\vec{r}, t)$ where \vec{d} is the induced dipole moment of the atom and $\vec{E}(\vec{r}, t)$ is the electric component of the light field.

³Rotating wave approximation: the Hamiltonian of the light-atom interaction exhibits two terms. One depends on $\delta = \omega_L - \omega_0$ and the other depends on $\omega_L + \omega_0$. The second term oscillates with a much higher frequency and therefore averages to zero on any appreciable time scale. This approximation is valid if the light frequency ω_L is close to the transition frequency ω_0 and if the intensity of the light is low so that the Rabi frequency is much lower than the transition frequency.

I/I_0 is the ratio between the laser intensity and the saturation intensity and $\vec{k}\vec{v}$ is the Doppler-shift of the transition of the moving atom.

Each photon carries a momentum $\hbar\vec{k}$ which is transmitted to the atom upon absorption. Through spontaneous emission a new photon will be emitted into an arbitrary direction. The momentum kicks of the photons from the spontaneous emission average to zero and only the transmitted momentum from the photons of the laser field remains. The atom experiences a net force in the direction of the laser propagation. This force is limited by induced emission. If the intensity of the light gets higher, induced emission happens more often. In an induced emission process an excited atom emits a photon in the direction of the light field, thus getting a momentum kick against the direction of the light field and no net force from absorption and emission occurs.

An important aspect to point out is that this force is velocity dependent because of the Doppler-shift. This is important because a velocity dependent force corresponds to a damping mechanism and thus a cooling effect emerges.

2.2. Trapping in momentum space

We now assume two counter-propagating lasers which are both red detuned with respect to the atomic transition ($\delta < 0$). We receive as for the total force in one dimension the equation

$$F(v) = \hbar k \frac{\Gamma}{2} \frac{\frac{I}{I_0}}{1 + \left[\frac{2(\delta - kv)}{\Gamma} \right]^2} - \hbar k \frac{\Gamma}{2} \frac{\frac{I}{I_0}}{1 + \left[\frac{2(\delta + kv)}{\Gamma} \right]^2}. \quad (2.2)$$

Through combination of Doppler shift and red detuning, atoms travelling towards a laser get their effective detuning reduced and scatter more photons. Because of this they receive a net force against their moving direction and are slowed down. If we extend this set-up to three dimensions it is called optical molasses which is described in depth in the paper of Lett et al. [23].

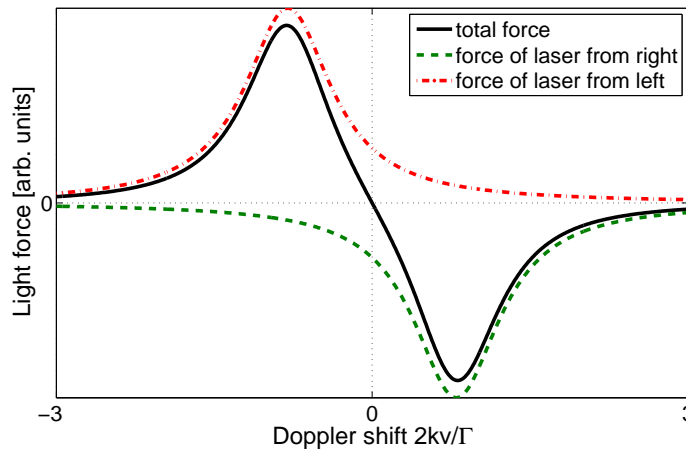


Figure 2.1.: Force on a moving atom in one dimension by two counter-propagating red-detuned lasers.

2.3. Doppler limit

With only the description above the atoms would soon reach temperatures of 0 K. Of course, this does not occur in reality. The above formula is based on mean values and does not take into account that light is quantised. Because of this quantisation the atoms momentum can only do hops of $\hbar k$ and the atom will perform a random walk in momentum space. In this random walk the square of the momentum does not vanish and constitutes a heating rate that counteracts the cooling. Taking heating and cooling into account the equilibrium temperature is given by the equation

$$M \langle v^2 \rangle = \frac{1}{2} k_B T = \frac{\hbar \Gamma}{4} \left(\frac{\Gamma}{-2\delta} + \frac{-2\delta}{\Gamma} \right), \quad (2.3)$$

where M is the mass of the atom species and k_B is the Boltzmann's constant. From this equation, the lowest achievable temperature should be obtained for a detuning $\delta = -\Gamma/2$. The temperature will then be

$$k_B T_{Doppler} = \frac{\hbar \Gamma}{2}. \quad (2.4)$$

For Rubidium this temperature is $T_{Doppler} \approx 140 \mu\text{K}$ and is called the Doppler limit. This corresponds to a velocity of the atoms of $v \approx 12 \text{ cm/s}$.

Measurements have shown even lower temperatures. This can not be explained with this simple scheme but is due to sub-Doppler cooling mechanisms such as Sisyphus cooling [24] or polarisation gradient cooling (details in section 2.6).

2.4. Trapping in real space

So far we have looked at how to slow atoms down, but they are not yet confined in space and can wander off. To confine them in space and make a MOT we use circular polarised red-detuned lasers and a linear magnetic field, therefore a constant magnetic field gradient which induces a spatially varying Zeeman splitting. For the explanation we again use a simplified one-dimensional model that can be extended to three dimensions and real atoms. We use a two-level atom with the lower level having a total spin of $F = 0$ and the excited level having a total spin of $F = 1$. For low magnetic fields these levels have a linear Zeeman splitting of their $2F + 1$ m_F -states. The ground state only has one $m_F = 0$ state and does not split at all. The excited state splits into its three $m_F = -1, 0, 1$ states (see Figure 2.2). We chose the Landé g-factor of our two-level atom in our model to be positive. Trapping also works for a negative g-factor by using the opposite circular polarisations.

The magnetic field relative to our chosen axis is zero at the centre, negative on the left side and positive on the right side. The laser from the left has σ^+ polarisation and therefore couples the ground state only with the $m_F = +1$ excited state. The laser from the right has σ^- polarisation and therefore couples the ground state only with the $m_F = -1$ excited state (see Figure 2.3).

Because of the red detuning δ compared to the atomic transition of the lasers the atoms left of the centre interact more with the laser from the left. Same applies to atoms on the right with the laser from the right. The atoms feel a net force that pushes them to the zero of the magnetic field.

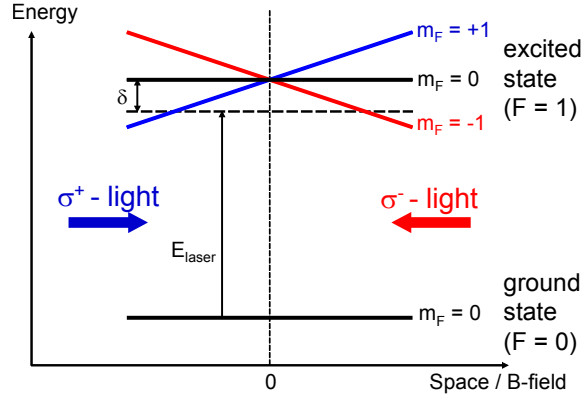


Figure 2.2.: Zeeman splitting of the $F = 1$ state puts the $m_F = \pm 1$ states to different energies at different positions in space. σ^+ - polarised light from the left is closer to resonance on the left side and σ^- - polarised light from the right is closer to resonance on the right side. Therefore the atoms experience a net force towards the centre of the MOT.

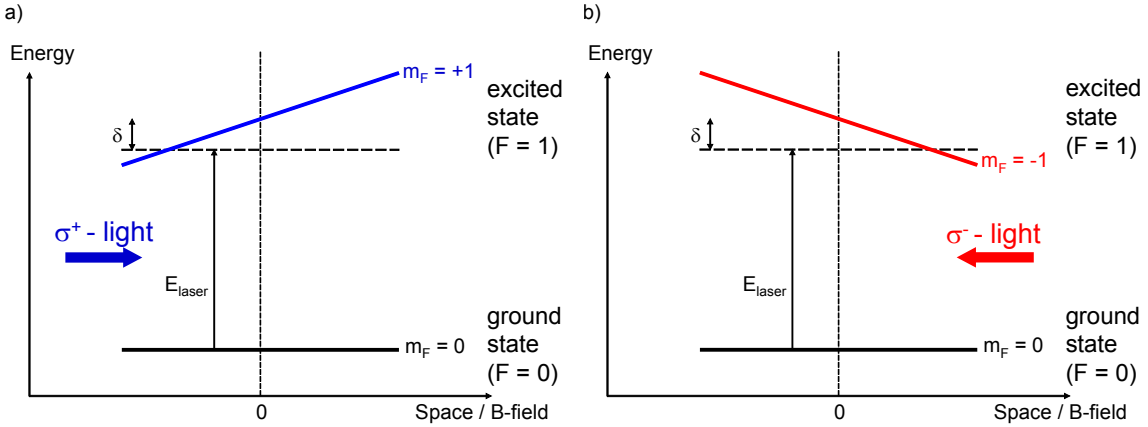


Figure 2.3.: States that are coupled by the laser from the left (a) and right (b) because of their distinct polarisation.

A magnetic set-up which can provide a constant magnetic field gradient along three axes is a quadrupole field generated by anti-Helmholtz coils.⁴

2.5. Six-beam MOT

The basic MOT consists of three counter-propagating pairs of laser beams. The polarisations in each pair are σ^+ and σ^- . The pairs are orthogonal to each other and are aligned with the axis of the magnetic quadrupole field.

A schematic of this basic MOT set-up can be seen in figure 2.4.

⁴Anti-Helmholtz coil: The geometry is similar to a Helmholtz coil but the current is passed in reversed direction in one of the coils. This generates two magnetic fields that point at each other and cancel in the middle. The field in the centre is in good approximation a quadrupole field with a constant field gradient.

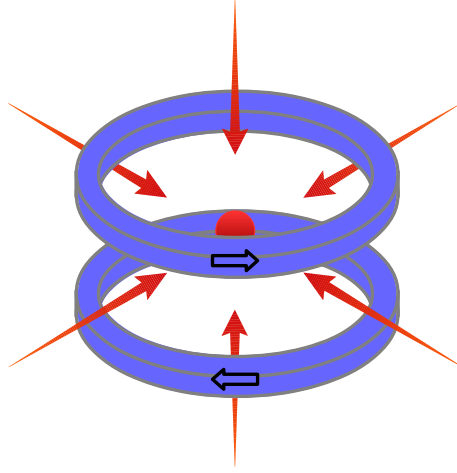


Figure 2.4.: Schematic of a six-beam MOT set-up.

2.6. Polarisation gradient cooling

In a MOT where the laser beams constitute of σ^+ and σ^- polarised light, polarisation gradient cooling is in effect. The standing wave made up by the two counter-propagating laser beams with polarisations σ^+ and σ^- has a linear polarisation that rotates in space over 2π in one wavelength. The atoms travelling in this rotating field have their quantisation axis turned. Since this is not instantaneous they always lag behind. Because of that the atoms travelling towards the σ^+ beam couple stronger to σ^+ light and scatter more photons from the σ^+ beam. Vice versa for the atoms travelling towards the σ^- beam. This effect is much stronger than the force from the Doppler-shift and thus leads to a stronger cooling effect. Details on this sub-Doppler cooling scheme can be found in the paper of Dalibard and Cohen-Tannoudji [24].

In the low-intensity limit the light shifts ΔE_g of the magnetic ground state is given by [22]

$$\Delta E_g = \frac{\hbar \delta \frac{I}{I_0} C_{ge}^2}{1 + \left(\frac{2\delta}{\Gamma}\right)^2}, \quad (2.5)$$

where C_{ge} is the Clebsch-Gordan coefficient which describes the interaction between the atom and the light field.

The final temperature reached with polarisation gradient cooling T_{lim} scales with the light shift of the ground state ΔE_g . It is describe by the equation

$$k_B T_{lim} = b \Delta E_g, \quad (2.6)$$

where b is a coefficient that describes which cooling scheme is used ($b = 0.125$ for Sisyphus cooling, $b = 0.097$ for the σ^+ and σ^- polarisation gradient cooling). From these equations one can see that lower temperatures can be reached by further detuning the lasers to the transition or by decreasing the power in the laser beams.

A limit for the lowest temperature achievable by laser cooling is the recoil temperature. It stems from the quantisation of the inertia $\hbar k$ that the photons carry and is

$$k_B T_{recoil} = \frac{\hbar^2 k^2}{M}, \quad (2.7)$$

where M is the mass of the atom. The recoil limit for ^{87}Rb is $\approx 0.36 \mu\text{K}$ which corresponds to a velocity of $\approx 8 \text{ mm/s}$.

2.7. Rubidium

Real atoms do not have only two energy levels but a huge amount of excitable levels. In our experiment we use Rubidium 87 (^{87}Rb) which is an alkali metal. Thus it has only one valence electron and therefore a quite simple energy level structure. Because of this it is possible to pick two states whose transition is far away from all other possible transitions and thus keeps excitation to other states to a minimum. The two levels that partake in the cooling transition for the MOT are $5^2\text{S}_{1/2}$ and $5^2\text{P}_{3/2}$. Because of the nuclear spin of ^{87}Rb these states have a hyperfine splitting. The $5^2\text{S}_{1/2}$ level splits in two states with $F = 1, 2$ and the $5^2\text{P}_{3/2}$ level splits into four states with $F = 0, 1, 2, 3$ (see Figure 2.5). For these dipole transitions the selection rules apply, therefore F can only change by ± 1 or 0 . Resulting from this the transitions $|5^2\text{S}_{1/2}, F = 2\rangle$ to $|5^2\text{P}_{3/2}, F = 0\rangle$ and $|5^2\text{S}_{1/2}, F = 1\rangle$ to $|5^2\text{P}_{3/2}, F = 3\rangle$ are forbidden.

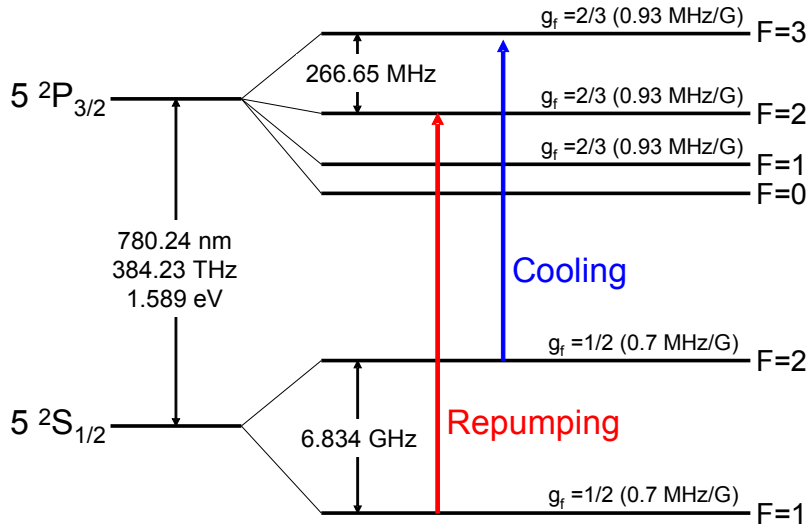


Figure 2.5.: Rubidium 87 D2 transition structure (adapted from [25]).

The transition we use as the two-level system for cooling and trapping is from $|5^2\text{S}_{1/2}, F = 2\rangle$ to $|5^2\text{P}_{3/2}, F = 3\rangle$.

2.8. Repumping

There is a small chance to excite an atom by the cooling laser into the $|5^2\text{P}_{3/2}, F = 2\rangle$ state. This state can decay via spontaneous emission into the $|5^2\text{S}_{1/2}, F = 2\rangle$ or $|5^2\text{S}_{1/2}, F = 1\rangle$ state. If it decays into the $|F = 1\rangle$ state this atom can not be excited by the cooling light any more, it has fallen into a so called “dark” state. To get these atoms back into the cooling cycle we need a second laser frequency. This repumping laser is resonant with the $|5^2\text{S}_{1/2}, F = 1\rangle$ to $|5^2\text{P}_{3/2}, F = 2\rangle$ transition. It excites the atoms into the $|5^2\text{P}_{3/2}, F = 2\rangle$ state until they fall into the $|5^2\text{S}_{1/2}, F = 2\rangle$ state and thus are back in the cooling cycle (see Figure 2.6).

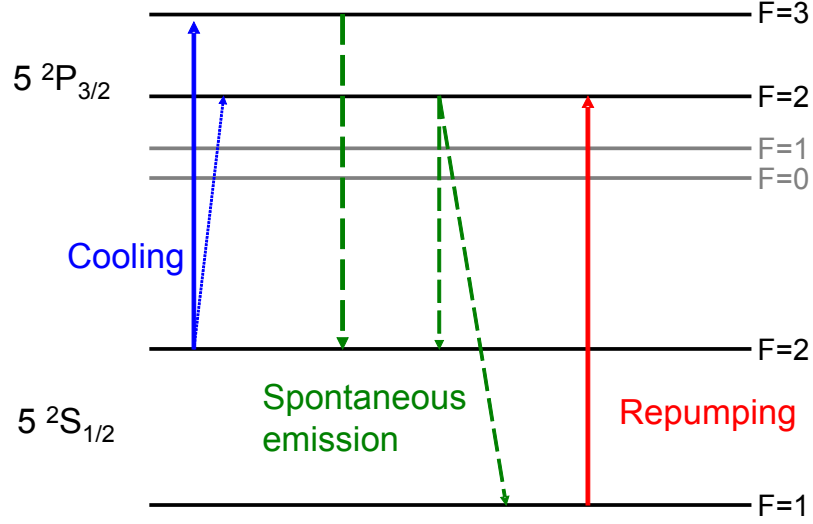


Figure 2.6.: Rubidium 87 MOT cycle: The small amount of atoms which are excited into the $|5^2P_{3/2}, F = 2\rangle$ state and decay into the $|5^2S_{1/2}, F = 1\rangle$ state are excited back into the $|5^2P_{3/2}, F = 2\rangle$ state by the repumping laser until they fall into the starting state $|5^2S_{1/2}, F = 2\rangle$.

2.9. MOT dynamics

The number of atoms in a MOT depending on time can be described by the equation [26]

$$\frac{dN}{dt} = R_f - \gamma N - \beta n^2 V. \quad (2.8)$$

Where N is the number of trapped atoms, R_f is the loading rate, γ is the loss rate due to collisions with the background gas, n is the density of the cloud of atoms, V is the volume of the cloud and $\beta n^2 V$ is the loss due to light induced collisions. The two dominant effects for these are fine-structure changing collisions and radiative redistribution. Details on these effects can be found in the article from Adams and Riis [26]. The gist of it is that both lead to a density dependent loss rate for the number of atoms in the cloud.

For the steady state the derivative is zero and the equation 2.8 simplifies to

$$0 = R_f - \gamma N - \beta N^2/V, \quad (2.9)$$

where we rewrote the last term by using $n = N/V$. For low background pressures the term $-\gamma N$ can be neglected. R_f is a constant and therefore we get the proportionality of the atomnumber in the steady state (where the MOT is saturated) $N \propto r^{3/2}$, where r is the radius of the cloud of atoms.

2.10. Temperature of a cloud of atoms

One can define the temperature as the mean of the kinetic energy

$$\frac{1}{2} k_B T = \langle E_k \rangle. \quad (2.10)$$

From a thermodynamics point of view defining a temperature for an isolated cloud of atoms is inappropriate. The system of atoms trapped by lasers is not in thermal equilibrium with its surrounding, which is a necessity to be able to define a thermodynamic temperature. Furthermore an infinite number of velocity distributions exist that have the same average kinetic energy but not the same temperature. For a cloud of cold atoms the velocity distribution is the Maxwell-Boltzmann distribution, hence the above definition of the temperature is still appropriate, convenient and widely used in the cold atoms field.

The time of flight (TOF) technique is one of the procedures for the measurement of this temperature and will be described in this section. In this technique multiple images of the same cloud of atoms (prepared in the same way) are taken after different times of evolution in free space. During this time of flight the cloud of atoms falls in the gravitational field and more importantly, expands according to its temperature. Because of the velocity distribution of the atoms, the MOT expands into a Gaussian shape. Measuring the size of the cloud of atoms at different times and fitting the corresponding sizes yields a numeric value for the temperature.

The size σ of the cloud of atoms is describe by the equation

$$\sigma(t) = \sqrt{\sigma_0^2 + \frac{k_B}{M}T \cdot t^2}, \quad (2.11)$$

where σ_0 is the initial size of the atom cloud, t is the time of flight and T is the temperature of the cloud of atoms. For easy fitting we square equation 2.11 and receive

$$\sigma^2(t^2) = \sigma_0^2 + \frac{k_B}{M}T \cdot t^2. \quad (2.12)$$

This equation is linear in the square of the time t and an easy linear fit can be performed by plotting the size squared dependent on the time of flight squared (see figure 2.7). The gradient of this fit corresponds to the temperature T .

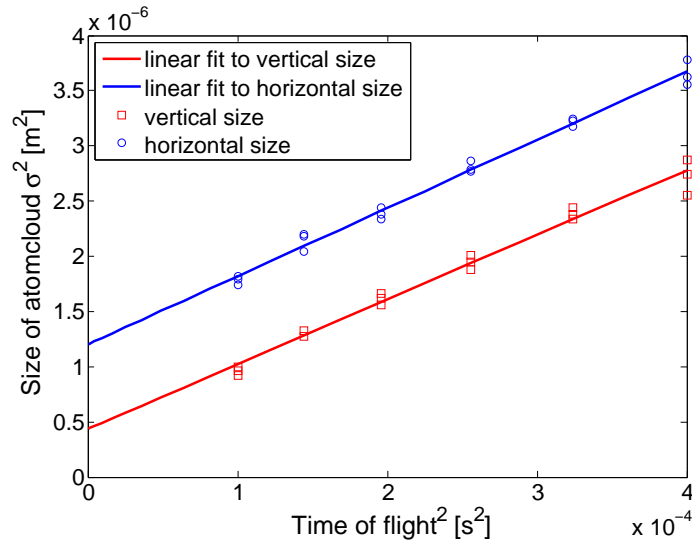


Figure 2.7.: Fits of the size of the cloud of atoms to determine the temperature. Both axes are squared so that the temperature is determined by a linear fit. The graph is from actual data from our experiment from section 4.2.8. The data points for the size stem from fitting a Gaussian to the image of the atom cloud. Lines: fits according to equation 2.12.

3. Experiment

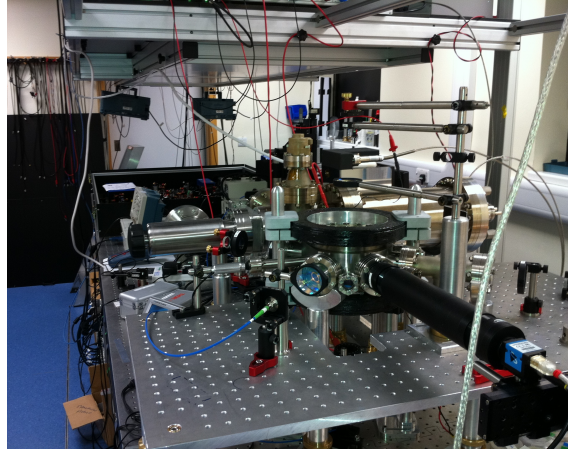


Figure 3.1.: Photo of the whole set-up.

This chapter describes the specifics of our MOT and the experimental set-up for the dual-colour MOT. It contains details on the vacuum system, magnetic fields, laser beams and the imaging system. Efforts put into realising the experimental conditions on which the theory depends are also described.

3.1. The MOT in our experiment

3.1.1. Reflection MOT

Although the future experiments will be using a five-beam MOT (see section 5.2), the measurements in this thesis were done on a six-beam retro-reflected MOT. A reflection MOT is similar to a six-beam MOT (see also section 2.5), where the counter-propagating laser beam of each pair is created by reflecting the first beam. To achieve the correct polarisation in the reflected beam a $\lambda/4$ -plate is placed in front of the mirror. Because the beam passes the $\lambda/4$ -plate twice its circular polarisation is turned into the other direction ($\sigma^+ \rightarrow \sigma^-$, $\sigma^- \rightarrow \sigma^+$).

An advantage of this set-up is the lower required laser power. Since three beams are reflected and therefore reused in the MOT, the laser power needed compared to the standard six-beam MOT is halved. A drawback in the reflection MOT is that the reflected beam has a little lower intensity in the centre of the MOT region because of absorption in the first beam by the atoms. This can cause asymmetries in the light forces and the resulting cloud of atoms, especially for very dense ones.

3.1.2. Dual-colour MOT

The speciality of our set-up - the dual-colour MOT - does not use a single frequency for the cooling laser but two frequencies close to each other (see Figure 3.2). The detunings of the lasers with respect to the resonance are named f_1 and f_2 throughout this thesis. The letter Δ is used to describe the difference between these two laser frequencies $\Delta = f_1 - f_2$ and we will call it relative detuning. A positive Δ denotes that f_2 is closer to the resonance of the transition. Details on the dual-colour MOT are given in section 4.1.

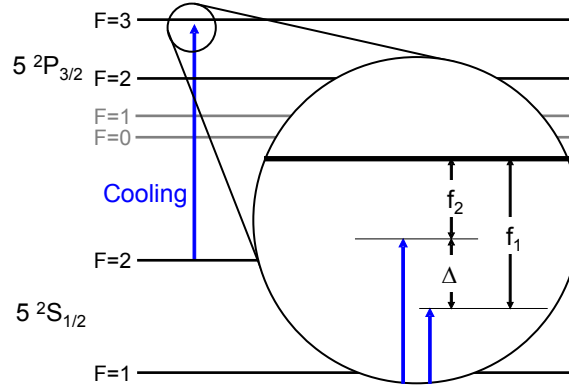


Figure 3.2.: ^{87}Rb cooling transition nomenclature for the two laser frequencies.

3.2. Set-up

3.2.1. Vacuum chamber

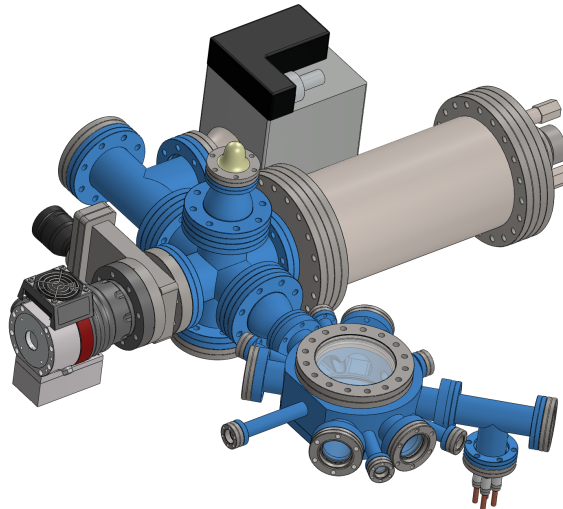


Figure 3.3.: Drawing of the set-up with the vacuum area highlighted.

Since we need a very good vacuum (between 10^{-10} mbar and 10^{-11} mbar), we need a high quality vacuum set-up. All the used components need to be specified for these low pressures. To achieve a vacuum of such magnitude it is necessary

to perform a bakeout. A bakeout is the process of heating all the high vacuum components to 100 °C–200 °C while pumping. This will get rid of outgassing of the components, adsorbed humidity and to some degree trapped air in pockets. The higher the bakeout temperature is chosen the faster this process will finish. One has to take precaution during heating and cooling to not be too fast and put strain on the components that might cause them to break. In our experiment we chose a bakeout temperature of 150 °C. With this temperature the bakeout of our vacuum set-up took a few days. The final pressure we were able to achieve is $\approx 8 \cdot 10^{-11}$ mbar.

The vacuum set-up consists of a few different parts and pumps which will be described in the following sections.

Experiment chamber

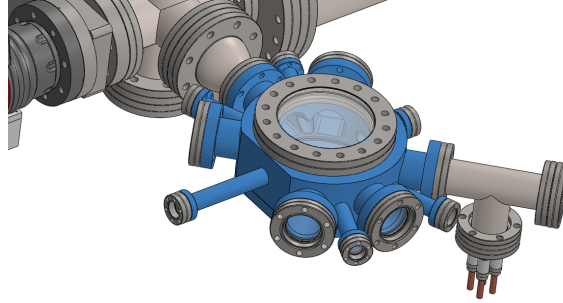


Figure 3.4.: Drawing of the set-up with the experiment chamber highlighted.

The experiment chamber is a special design by our group, it has been manufactured by a specialised company¹ and can be seen in figure 3.4. The design takes a lot of cold atom experiment needs into consideration and is therefore quite flexible. It has six large (CF40) viewports with special coated windows that have the whole glass area coated and therefore a bigger usable area than normal viewports. An additional two small (CF16) viewports are in the same central plane. These ports allow, by the set-up of a magnetic transport to turn the chamber into a pre-chamber for future experimental set-ups. Four small (CF16) viewports are located in a plane a few mm below the centre with which the atoms can be observed after a time of flight. For example light sheet imaging would be possible with these viewports. At the top resides a very large (CF100) viewport. The mounting for future experiments will be connected to the chamber in the position of this viewport. Attached at the bottom is a special viewport with a slanted inner border for better optical access. This viewport is not mounted by a CF-seal but a special Helicoflex sealing.

Ion pump

The ion pump² (pink arrow in picture 3.5) is the main pump after achieving UHV. It ionises atoms and accelerates them with an electric field onto a surface and traps them there.

¹Torr scientific Limited (www.torrscientific.co.uk).

²Vaclon Plus 55 Star Cell (50l/s), Agilent Technologies (www.agilent.com).

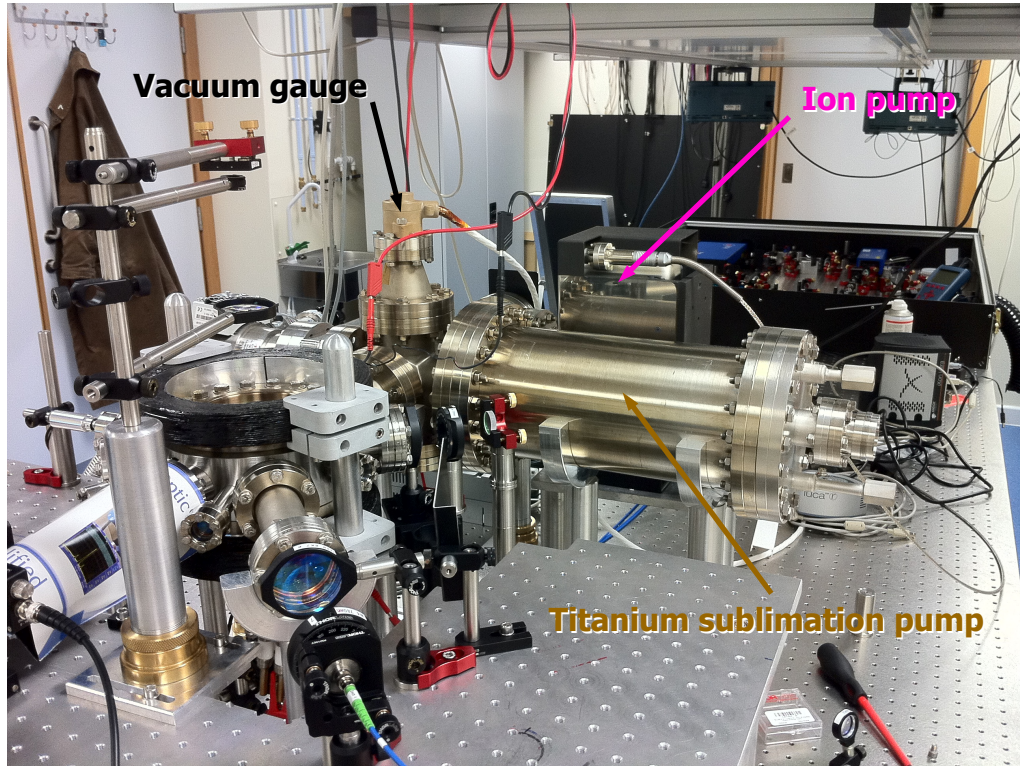


Figure 3.5.: Photo of set-up with the pumps in good sight.

Ti-Sb pump

The titanium sublimation pump³ (brown arrow in picture 3.5) is used only for very low pressures. It works by evaporating titanium onto a large surface area. Since titanium is a very good absorbent, gas atoms and molecules stick to the coated surface. The evaporation is done by heating a dispenser inside the pump. This is done every few days or weeks, depending on the background pressure.

Turbopump

The turbopump⁴ is only used to pump down and is afterwards detached from the set-up. Between turbo pump and vacuum set-up is an angle valve that meets the imperviousness needs. Prior to the turbopump is a roughing pump that provides the pre-vacuum needed by the turbopump. The turbopump has slanted rotor blades inside which rotate at a very high speed (≈ 1500 rpm). These blades hit the atoms and push them away from the low pressure side.

Vacuum gauge

The vacuum gauge⁵ is used to measure (estimate) the pressure in the vacuum chamber. It works by ionising atoms, collecting them and measuring the occurring current. This current is related to the background pressure. At very low pressures

³Titanium Sublimation Cartridge 916-0050, Agilent Technologies (www.agilent.com).

⁴HiPace 80, Pfeiffer Vacuum (www.pfeiffer-vacuum.com).

⁵UHV-24 Bayard-Alpert Gauge Tube, Agilent Technologies (www.agilent.com).

(below 10^{-10} mbar) this gauge does not work reliably any more and the displayed value has to be treated as an estimate and not as a calibrated value.

Rubidium Dispenser

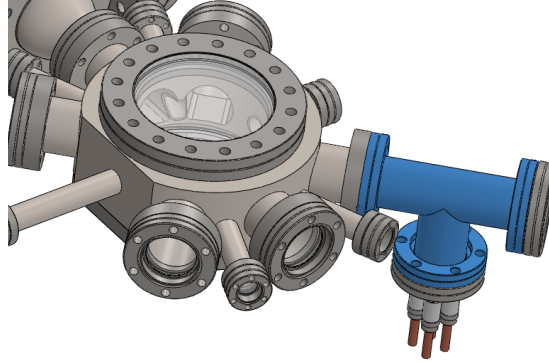


Figure 3.6.: Drawing of the set-up with the dispenser area highlighted.

Positioned close to the experiment chamber, mounted on an electrical feedthrough is the Rubidium dispenser⁶ (see picture 3.6). This dispenser contains a Rubidium salt and can be heated by applying a current through it. The composition of the Rubidium isotopes in the salt is 72 % ^{85}Rb and only 28 % ^{87}Rb . This composition stems from the stability of the isotopes. ^{85}Rb is stable and ^{87}Rb has a half-life time of $4.9 \cdot 10^{10}$ years. All other Rubidium isotopes have half-life times in the range of weeks or much shorter. Since we only trap ^{87}Rb the ^{85}Rb atoms are detrimental by increasing the background pressure.

When the dispenser is heated the salt emits Rubidium at an almost constant rate. By controlling the current through the dispenser we can control its temperature and therefore the rate of emitted Rubidium and the background pressure in the chamber. The majority of the measurements have been conducted at a dispenser current of 3 A which translates to a background pressure of $\approx 9 \cdot 10^{-11}$ mbar.

3.2.2. Quadrupole Coils

The magnetic field for our MOT is provided by two coils in anti-Helmholtz configuration (see blue arrow in picture 3.7). The coils are an inheritance from a former experiment and were spooled by hand. With a current of 3 A in each coil we achieve a magnetic field gradient of ≈ 7.9 G/cm in the strong axis. We chose to provide the currents to the two coils not by a single source but by two channels of a power supply. This allows us to unbalance the currents in the coils and therefore we can adjust the vertical position of the point of zero magnetic field and thus the vertical position of the MOT.

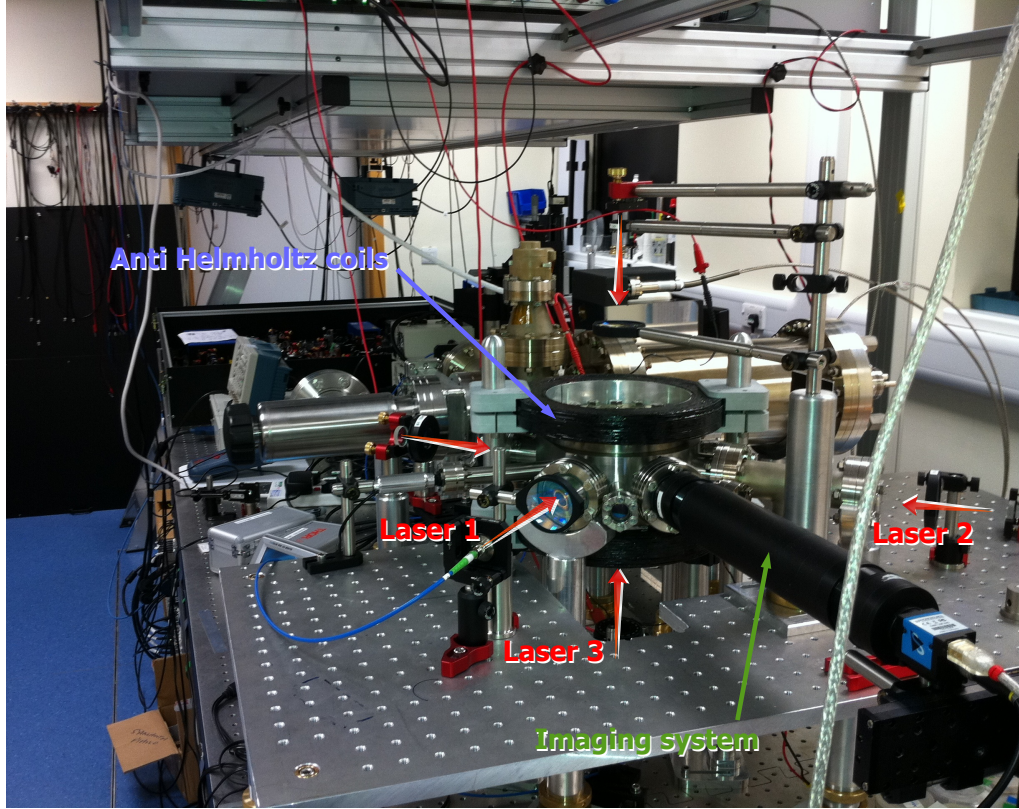


Figure 3.7.: Photo of the set-up with laser beams indicated.

3.2.3. Laser set-up

A schematic of our laser set-up can be seen in figure 3.9. We have two laser sources the DL pro⁷ and the TA pro.⁸ Both lasers are operated at 780 nm and are frequency locked with the aid of Rubidium vapour cells by Doppler free absorption spectroscopy. The DL pro is locked onto the $F_{1 \rightarrow 1}$ transition and afterwards shifted by an acousto-optical modulator (AOM)⁹ by 156.9 MHz in a double-pass set-up. After the AOM the laser from the DL pro is resonant to the transition $|5^2S_{1/2}, F = 1\rangle$ to $|5^2P_{3/2}, F = 2\rangle$ which is used for repumping. The master laser of the TA pro is shifted by 107 MHz by an AOM and locked onto the $F_{2 \rightarrow 2,3}$ crossover transition. Prior to the AOM the beam is split and the majority of the power is fed into the tapered amplifier. The laser exiting the TA pro is shifted by -240 MHz from the transition $|5^2S_{1/2}, F = 2\rangle$ to $|5^2P_{3/2}, F = 3\rangle$.

The laser from the TA pro is split a few times and used for the two cooling frequencies f_1, f_2 , imaging and optical pumping. The laser from the DL pro is only used for repumping.

Following is a brief description of the further light preparation (see also figure 3.9). The laser beam from the TA pro is split with the aid of a polarising beam splitter (PBS). The two beams are shifted to the desired frequencies f_1, f_2 by AOMs in

⁶Alkali metal dispensers, SAES Getters (www.saesgetters.com).

⁷Diode laser, TOPTICA Photonics AG (www.toptica.com).

⁸Diode laser with tapered amplifier, TOPTICA Photonics AG (www.toptica.com).

⁹AOM: Acousto-optical modulator, diffracts a laser and shifts its frequency with acoustic waves in a crystal.



Figure 3.8.: Photo of the laser table.

a double-pass set-up. This double-pass set-up is important because changing the frequency with the AOM also changes the deflection angle from the AOM. With the double-pass set-up this angle is the same on the way back and the resulting beam does not change its position when the frequency of the AOM is changed. The first laser is further split to supplement light for imaging and optical pumping (not used in this thesis as magnetic trapping is not yet implemented). The two lasers for imaging and optical pumping are recombined using a PBS and coupled into a fibre. The repumping laser from the DL pro and the two cooling lasers are superposed and split into three beams with the same relative intensities by a clever combination of PBS and $\lambda/2$ -plates. These three beams are coupled into fibres and form the reflection MOT at the vacuum chamber.

Telescopes and prisms at fitting locations shape the beams and assure a coupling to the mode of the fibres. Shutters are in appropriate locations to ensure safety and to shut light completely off when needed in the experiment.

A typical laser power in each beam at the experiment chamber is ≈ 32 mW. With a laser beam diameter of ≈ 2 cm this corresponds to intensities of ≈ 10 mW/cm² in each beam.

3.2.4. Imaging system

Our imaging system consist of a camera¹⁰ and two lenses¹¹ which are connected by lens tubes. The first lens has a focal length of $f_1 = 150$ mm and is positioned close to a window of the experiment chamber, 150 mm $= f_1$ from the centre of the chamber away. The second lens with a focal length of $f_2 = 75$ mm is 225 mm $= f_1 + f_2$ after the first lens. The camera is distanced in a way that the CCD sensor of the camera is 75 mm $= f_2$ from the second lens.

This set-up ensures that the imaging system can be used for fluorescence imaging and absorption imaging without any adjustments.

The magnification of the lens system is $1/2$. With the area of the CCD of 6×8 mm²

¹⁰DMK 23F445, The Imaging Source Europe GmbH (www.theimagingsource.com).

¹¹Achromatic doublets: Achromatic double lenses AC508-075-B-ML and AC508-150-B-ML by Thorlabs Inc. (www.thorlabs.com).

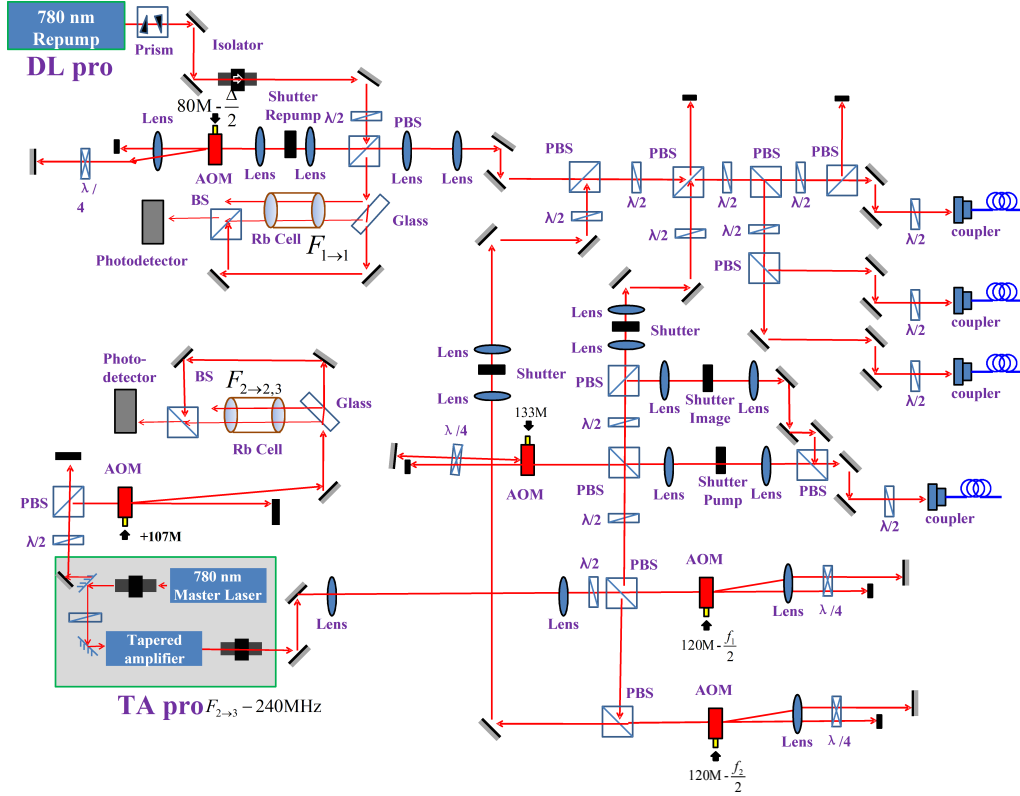


Figure 3.9.: Schematic of our laser set-up. See text for details.

we can image an area of $12 \times 16 \text{ mm}^2$. The resolution of the camera is 1280×960 pixels, hence each pixel corresponds to a length of $12.5 \mu\text{m}$ in object space.

4. Dual-colour MOT

4.1. Introduction

This chapter describes the conducted measurements on the dual-colour MOT and the conclusions we can draw from the data. The measurements are still ongoing during the time this thesis is written. We do show that we can achieve considerably higher atom numbers (up to a factor of four) than with a single-colour set-up while still keeping the temperature of the atom cloud the same ($\approx 100 \mu\text{K}$).

“Dual-colour” means that we are using two frequencies that are only a few MHz apart instead of a single frequency. The nomenclature that is used can be seen in figure 4.1. Typical values for the dual-colour MOT are $f_1 = -24.3 \text{ MHz}$, $f_2 = -20.7 \text{ MHz}$ and therefore $\Delta = -3.6 \text{ MHz}$.

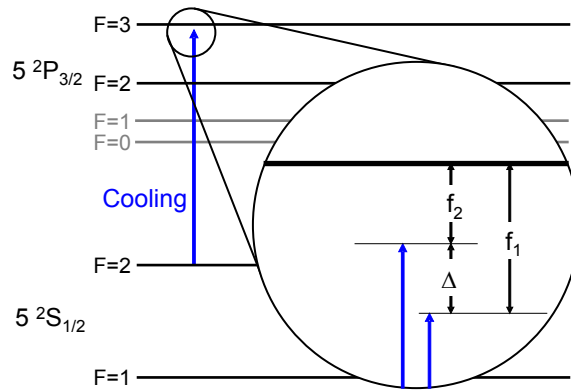


Figure 4.1.: ^{87}Rb cooling transition nomenclature for the two laser frequencies.

Similar experiments with rubidium have been conducted by Sinclair, Riis and Snadden [20] and Cao, Luo, Wang, Chen and Wang [21]. Sinclair et al. used an opaque spot to block the centre part of the laser beam of one frequency. Cao et al. used two different beam diameters for the two different frequency laser beams. Both experiments achieve a higher number of atoms than in the respective single-colour case. They relate the increase of atom number to a larger spatial size of the MOT, therefore a reduced density and lower density-induced losses (see also section 2.9). An explanation for why the MOT is larger in size is not given. Pradhan, Gaur, Manohar and Jagatap [27] have achieved a higher number of caesium atoms in a MOT by using a near resonant control laser that does not overlap with the MOT region but a small fraction of the capture region.

Our set-up is simpler than the ones mentioned above because our two laser beams have the same spatial mode, therefore alignment of the beams relative to each other is not a concern. They are overlapped on the laser table and then coupled into single-mode polarisation maintaining fibres with the same polarisation. The fibres lead the light to the experiment where the laser beams are enlarged to the desired

size and the correct circular polarisation is induced by $\lambda/4$ -plates. The two frequency laser beams share the same single-mode polarisation maintaining fibres and therefore share the same spatial mode at the experiment.

4.2. Measurements

4.2.1. Overview

Describing all measurements would go beyond the scope of this thesis. Hence this section contains only the most interesting measurements on the dual-colour MOT in chronological order.

At first we did necessary calibration measurements to figure out the peculiarities of the set-up and to get a feeling for what parameter ranges are interesting and convenient to work with. The parameters we found are frequencies f_1, f_2 around 24 MHz and relative detunings Δ of a few MHz, the background pressure in the region of $1 \cdot 10^{-10}$ mbar, the magnetic field gradient in the strong direction at ≈ 8 G/cm ($1 \text{ G} = 0.1 \text{ mT}$), the laser power around 30 mW in each laser beam which corresponds to an intensity of $\approx 10 \text{ mW/cm}^2$ and a loading time of roughly 10 s.

Next we did experiments on the dual-colour MOT and scanned the frequencies f_1 and f_2 to achieve a high number of atoms ($\approx 2 \cdot 10^8$) at a fairly low background pressure ($\approx 9 \cdot 10^{-11}$ mbar). We saw that the MOT did not have a nice Gaussian shape hence preventing fitting and thermometry. We accomplished to get the MOT into a Gaussian shape with a special procedure. From that point on we could determine the temperature of the cloud of atoms by fits to absorption images of the atom cloud after different times of flight.

After that we looked at the number of atoms after different loading times and found that the dual-colour MOT has twice the atom number compared with the single-colour MOT after only 10 s of loading and has four times the number of atoms in saturation.

In the later measurements we investigated the temperature of the cloud of atoms. We managed to reach temperatures of 100 μK for both the single-colour and the dual-colour MOT.

4.2.2. Calibration and test measurements

One of the very first measurements on the set-up was a comparison between a five-beam MOT and a six-beam MOT. The six-beam MOT is the MOT we use for all our experiments and uses three counter-reflected beams by guiding them through a $\lambda/4$ -plate and reflecting them on a mirror. The five-beam MOT demonstrates that a MOT is possible with a reflection coated $\lambda/4$ -plate. We used a gold coated $\lambda/4$ -plate to reflect the vertical beam instead of a combination of a normal $\lambda/4$ -plate and a mirror. In the future experiments such a coated $\lambda/4$ -plate will reside inside the vacuum chamber on the mounting, for this test it was mounted outside the chamber.

These measurements were done with only one frequency and we also tested out different magnetic field gradients. Since this is a very early measurement in the lifetime of the set-up no imaging system or experimental control was installed. We

measured the atomnumber by fluorescence with a Si-photodetector¹ by focusing an image of the MOT with a lens onto the active area of the photodetector. One can determine the number of atoms N by fluorescence with the equations:

$$N = \frac{P_{tot}}{h\nu \cdot \Gamma_{scat}} \quad (4.1)$$

$$P_{tot} = P_{PD}/\Omega \quad (4.2)$$

$$P_{PD} = V_{PD} \cdot R(\lambda) \cdot R_{load} \quad (4.3)$$

$$\Gamma_{scat} = \frac{\left(\frac{I}{I_S}\right) \cdot \pi \cdot \Gamma}{1 + \left(\frac{I}{I_S}\right) + 4 \left(\frac{\delta}{\Gamma}\right)^2} \quad (4.4)$$

Where P_{tot} is the total power emitted by the atom, Ω is the solid angle between the atom and the lens area, P_{PD} is the Power impinging on the Photodetector, $R(\lambda)$ is the spectral efficiency of the detector and R_{load} is the shunt resistor on which the voltage V_{PD} is measured. ν is the frequency of the laser light. Γ_{scat} is the scattering rate of photons by the atom, I is the total laser intensity, I_S is the saturation intensity (which is different for different polarisations and a common value that has been determined by comparing results and was used in this calculations is $I_S = 4.1 \text{ mW/cm}^2$). Γ is the natural line width of the transition, for the cooling transition in ^{87}Rb this is $2\pi \times 6 \text{ MHz}$ and δ is the detuning of the laser light with respect to the cooling transition.

Together these equations describe the number of atoms N depending on the Voltage from the photodetector V_{PD} and the detuning δ . Using these equations we calculate an estimation for the number of atoms in the MOT. The results can be seen in figure 4.2. Each data point is an average over a few seconds of the fluorescence value. Further statistics are not involved in this measurement.

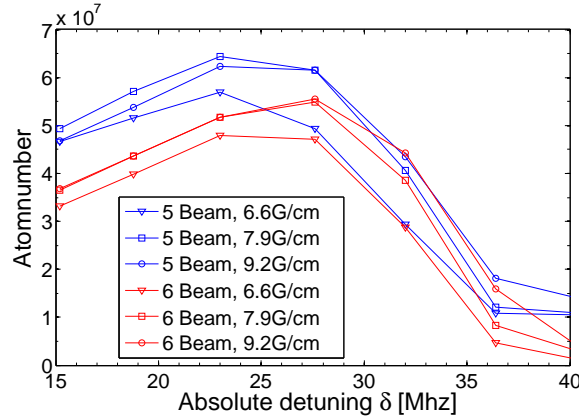


Figure 4.2.: One of the first measurements of a single-colour MOT in our chamber. Comparison between five-beam MOT and six-beam MOT at different magnetic field gradients.

This measurement was one of the first tests to see what ranges we will have to expect for our experiment parameters. It proved that the five-beam MOT is possible with our gold coated $\lambda/4$ -plate.

¹High-speed photodetector DET36A, Thorlabs Inc. (www.thorlabs.com).

4.2.3. First dual-colour MOTs

One of the early measurements on the dual-colour MOT is depicted in figure 4.3. Each picture represents an absorption image of the dual-colour MOT after 10s of loading from a background pressure of $\approx 9 \cdot 10^{-11}$ mbar. The images were taken after a time of flight² (TOF) of 4 ms. Frequencies f_1 , f_2 and therefore also Δ were kept constant throughout the loading cycle (naming convention as described in section 4.1). Frequency f_1 was scanned from -13.1 MHz to -30.9 MHz in nine steps (2.2 MHz step size), the relative detuning Δ was scanned from $+4.5$ MHz to -4.5 MHz in eleven steps (0.9 MHz step size). Since we have double-pass set-ups for our AOMs the laser beams do not move when changing the frequencies and fibre coupling stays the same. Thus the laser power is roughly the same throughout these measurements. Only the frequency dependent efficiency of the AOMs changes the laser power slightly. The laser power in each beam is ≈ 32 mW. With the beam size of ≈ 2 cm this corresponds to intensities of ≈ 10 mW/cm² in each beam.

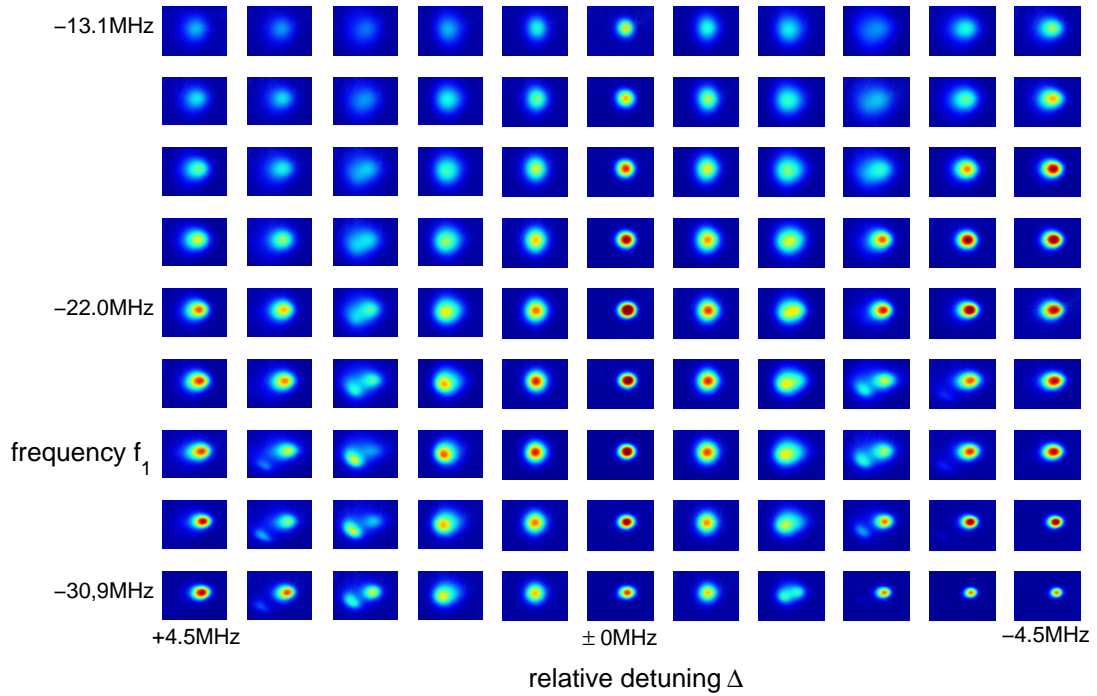


Figure 4.3.: Absorption images of MOTs: single-colour case in the middle column, the rest are dual-colour MOTs with different relative detuning Δ .

Three full measurement runs were conducted, depicted in the figure are the pictures of one full run. The other runs gave the same results. There is a little redundancy in these measurements because the laser beams of f_1 and $f_2 = f_1 - \Delta$ have the same spatial mode and closely the same power. Switching f_1 and $f_2 = f_1 - \Delta$ results in the same picture. Hence the picture of f_{1a}, Δ_a is similar to the picture of $f_{1b} = f_{1a} + \Delta_a, \Delta_b = -\Delta_a$.

Our primary goal with this measurement was to receive atom numbers depending on the frequency f_1 and the relative detuning Δ . Instead what we saw in this ex-

²Time of flight (TOF): the time between turning off the trap and taking the image. During this time the cloud of cold atoms expands according to its temperature and falls down due to gravity.

periment is that the MOT changes shape and even splits depending on the relative detuning Δ . This was unexpected because the shape of the MOT should be determined by the magnetic field as discussed in section 2.4 which is certainly close to a quadrupole field. Hence the MOT should be Gaussian. We do not yet understand why we get these split atom clouds and the standard theory can not describe the effect. High atom numbers are achieved particularly at the parameter regime where the MOT becomes deformed, grows in area and even splits in two. The respective relative detuning Δ is $\approx \pm 3.2$ MHz. Sinclair et al. [20] also see an atypical shape of their MOT in the dual-colour case which they did not understand. Important to note is that this splitting is not dependent on the absolute frequencies f_1, f_2 but only on the relative detuning Δ between the two. The single-colour case ($\Delta = 0$) is the middle column of pictures and it shows no splitting or unexpected effects. Therefore it adheres to the theory from section 2.4.

The increase in the number of atoms can be explained by an increase in volume of the cloud of atoms and therefore a reduced density. The main loss mechanism for large atom clouds is density dependent (see theory in section 2.9), hence a lower density in a larger volume gives a higher total number of atoms.

4.2.4. Getting the MOT in shape

For precise measurements of the temperature of the atoms it is desirable for the atom cloud to be Gaussian so we can make an easy fit and determine temperature by fitting to the size of the cloud of atoms after different times of flight. Additionally it will increase our precision in determining the number of atoms. There are other ways to determine the number of atoms like integrating over the optical density of the image and relating it to the total number of atoms. This method is also implemented in our evaluation and works for any shape of the atom cloud, but in our case it is not as precise as fitting a Gaussian. The integration method was used in the previous measurement.

We attain a Gaussian shape of the atom clouds this with a special procedure: During the last 5 ms of the loading cycle we set the relative detuning Δ to zero (f_2 is set to the value of f_1) and therefore have a normal single-colour MOT. The shape of the atom cloud becomes almost Gaussian. A comparison of two pictures of this experiment run with the short single-colour MOT at the end of the loading cycle and the previous run with the same parameters can be seen in Figure 4.4. Because this procedure works very fast compared to the MOT loading time the total atom number is not affected. The parameters (background pressure, loading time, etc.) of the measurement were the same as in the previous one. Another benefit of this technique is that the temperature of the cloud is also reduced and therefore images with longer TOF can be taken without the cloud becoming larger than the CCD sensor. Further discussion on the temperature of the atom cloud will be presented in section 4.2.8.

After figuring out this special procedure we are able to receive proper data on our temperature and a more precise number of atoms.

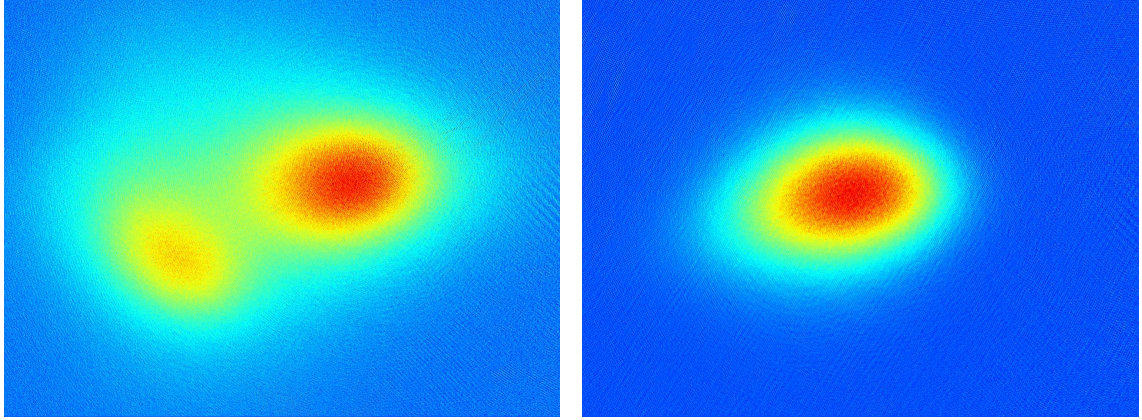


Figure 4.4.: Comparison of the dual-colour MOT with the procedure of the short single-colour MOT at the end of loading (right) and without (left). Both images map an area of $6 \times 8 \text{ mm}^2$. Parameters: $f_1 = 24.3 \text{ MHz}$, $\Delta = -2.7 \text{ MHz}$, time of flight = 4 ms.

4.2.5. Scanning the frequency domain

Next we did an overview measurement over the interesting frequency region with a small step size for the scanned parameters (f_1 , Δ). The experiment cycle was kept the same with the short single-colour MOT at the end of loading. The loading time was increased to 15 s. Background pressure was the same at $\approx 9 \cdot 10^{-11} \text{ mbar}$. The frequency f_1 was scanned from -13.1 MHz to -30.9 MHz in nine steps (2.2 MHz step size), the relative detuning Δ was scanned from $+8.9 \text{ MHz}$ to -8.9 MHz in 21 steps (0.9 MHz step size). The results of this measurement can be seen in figure 4.5. Three complete runs of the measurements were performed and the numbers plotted are the average over these three runs.

One can easily see that in the single-colour case ($\Delta = 0$, the valley in the middle) the atom numbers are significantly lower up to a factor of 2.5. Highest atom numbers are achieved in the region where $\Delta = \pm 3.6 \text{ MHz}$.

For further investigations we kept frequency f_1 constant at 24.3 MHz and focused on changes induced due to changes in the relative detuning Δ .

4.2.6. Loading

Loading times

Next we investigated MOT loading times as a function of the relative detuning Δ . In cold atoms experiments the loading time of the MOT is often a large fraction of the whole experiment cycle. Therefore keeping the loading time short greatly improves the rate of experiment runs. In the measurements we looked at the atom number after different loading times for different values of the relative detuning Δ (see figure 4.6). The figure on the left depicts a scan over different relative detunings as an overview. The figure on the right shows more detailed measurements of the single-colour case ($\Delta = 0$) and the optimal dual-colour case ($\Delta = -3.6 \text{ MHz}$). Background pressure and magnetic field gradient were kept the same as the previous measurements. In the measurement depicted on the left the relative detuning Δ was

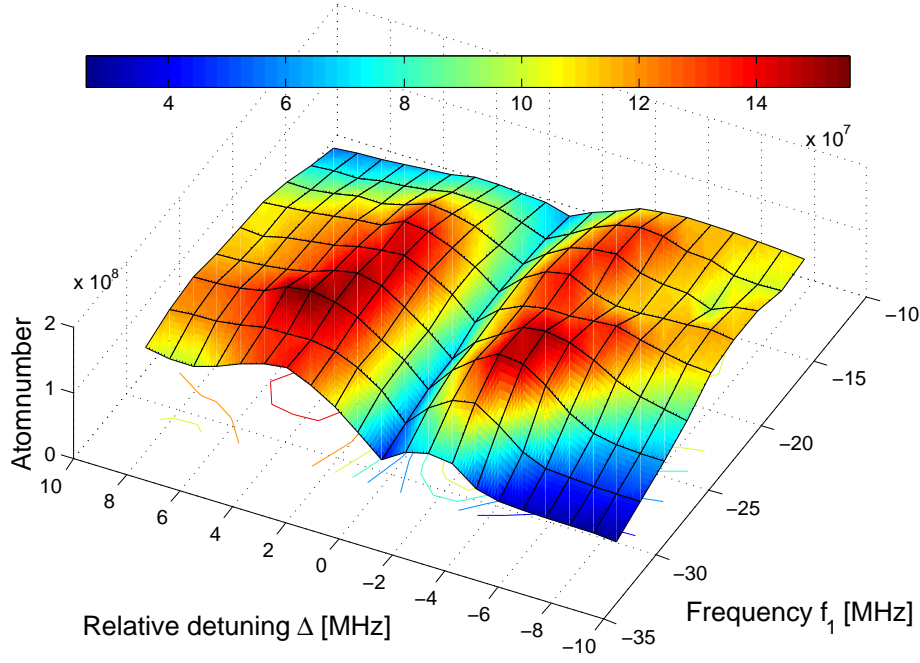


Figure 4.5.: Atom numbers depending on frequency f_1 and relative detuning Δ .

scanned from +8.9 MHz to −8.9 MHz in 21 steps (0.9 MHz step size) and the loading time was scanned from 15 s to 95 s in five steps (20 s step size). The measurement shown on the right uses 0 and −3.6 MHz for the relative detuning Δ and a smaller step size for the loading time (parameter range from 5 s to 100 s in 20 steps with a stepsize of 5 s). Both experiments were conducted with three experiment runs. Depicted is the average of the three runs. The error bars in the right image stem from this averaging.

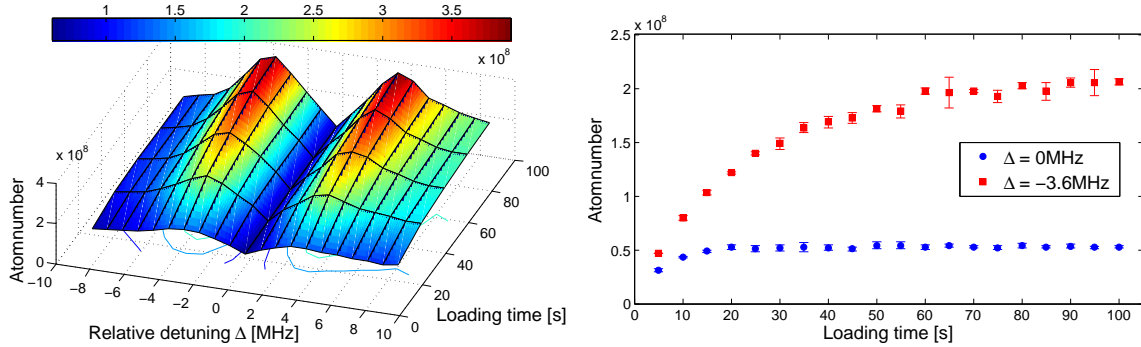


Figure 4.6.: Atom numbers depending on loading time and relative detuning Δ . Frequency f_1 is constant at 24.3 MHz. The left figure is an overview. The right figure depicts more precise measurements and a comparison between the single-colour case ($\Delta = 0$) and the dual-colour case ($\Delta = -3.6$ MHz).

The symmetry in the image on the left is a good indication of the importance of the value of the relative detuning Δ on the performance of the dual-colour MOT. The two peaks in the number of atoms are at frequencies 20.7 MHz, 24.3 MHz and 24.3 MHz, 27.9 MHz. Their number of atoms differs only slightly but the number of

atoms differs greatly with changes in the relative detuning Δ .

It seems that initially the dual-colour MOT does not load faster but it takes much longer to saturate. Therefore we have twice the number of atoms compared to the single-colour MOT after only 10s of loading. For high loading times of over 1 min we get four times the number of atoms compared to the single colour MOT.

Since the dual-colour MOT can hold much more atoms than the single-colour MOT but takes a long time to saturate it might be a good idea to load it with a different loading scheme. A 2D-MOT or a Zeeman slower might be good ways to fill the dual-colour MOT to saturation in a much shorter time.

All the papers mentioned in the introduction [20] [21] [27] contain a similar measurement where they observe similar results.

Loading characteristics

Further investigation on loading characteristics were conducted by looking at the fluorescence signal during the MOT loading process. A fit to these curves delivers the characteristic loading time τ .

The number of atoms during the loading process can be well approximated by the equation

$$N(t) = N_{max} \cdot \left(1 - e^{-\frac{t}{\tau}}\right), \quad (4.5)$$

where N_{max} is the atom number in saturation. For each data point in figure 4.7 the fluorescence signal during MOT loading for 30s was recorded. Fitting of the equation above delivered the values for the figure. Determining the atom number in the same way as in section 4.2.2 is not possible because the lasers have two frequencies. Hence equation 4.2.2 can not be applied and we do not know the exact scattering rate. Background pressure and magnetic field gradient were kept the same as the previous measurements again. The relative detuning Δ was scanned from +8.9 MHz to -8.9 MHz in eleven steps (1.8 MHz step size). Only one run was conducted but the fits to the fluorescence match the data very well.

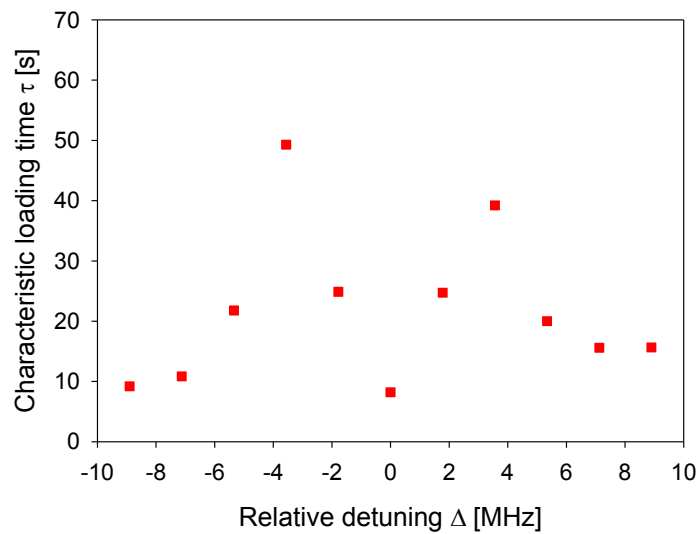


Figure 4.7.: Characteristic loading time τ depending on relative detuning Δ .

The characteristic time τ for the single-colour MOT is only 8.2s, for the dual-colour MOT it gets as high as 49s. We see from this experiment that the dual-colour

MOT loads for much longer times and which is the reason why it reaches a higher number of atoms. This measurement is consistent with the previous one.

4.2.7. Power ratios

The next question we investigated was whether changing the power ratios between the two frequencies f_1, f_2 has an impact on the MOT. For this we changed the power in the laser beams of the two frequencies by adjusting the polarisation with $\lambda/2$ -plates in front of the polarising beam splitters that combine the beams. Depending on the polarisation of the laser beam a different amount of light is guided towards the experiment by the polarising beam splitter, the rest is absorbed by a beam block. Since we wanted to keep the total power constant we had to use only half the total power to be able to scan the whole range of ratios. The loading time for these measurements was 15 s. Parameters for the frequencies were $f_1 = 24.3$ MHz and relative detuning $\Delta = -3.6$ MHz. The result is depicted in figure 4.8. Three experiment runs were done and the average numbers of these three runs are plotted. The error bars stem from this averaging.

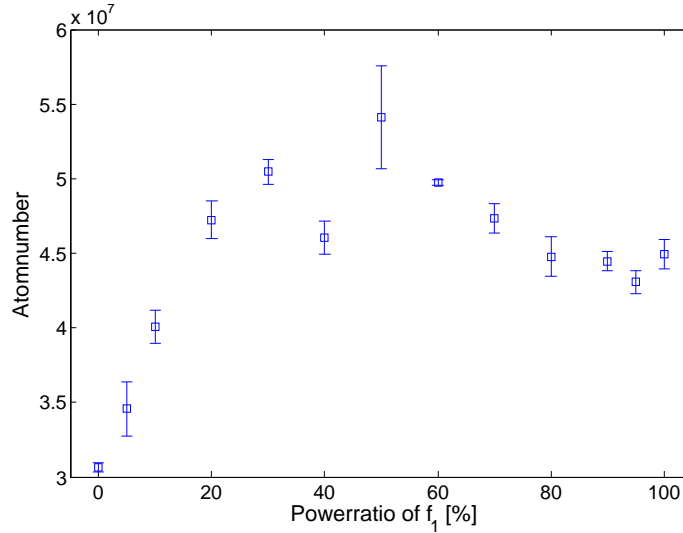


Figure 4.8.: Atom numbers depending on power ratios in the two frequencies. Total power is kept constant, frequency $f_1 = 24.3$ MHz and relative detuning $\Delta = -3.6$ MHz.

The measurements indicate that deviating from a 50/50 distribution is detrimental to the number of atoms of the dual-colour MOT. Our further experiments were done with the same power in both frequencies because of this result.

4.2.8. Temperature

A common technique to get atom clouds to low temperatures is moving the cooling frequency (f_1) to further red detuning with respect to the transition and decreasing the power in the laser beam as discussed in section 2.10. We use this technique at the end of our MOT cycle after the short single-colour MOT. The frequencies f_1 and f_2 which are set equal during the last few ms of the experiment due to the reasons given in section 4.2.4 are set to a detuning of 75.4 MHz with respect to the

transition for 1 ms. By changing the frequencies this far the efficiency of the AOMs is lowered and therefore the laser power is also reduced. Measurements can be seen in figure 4.9.

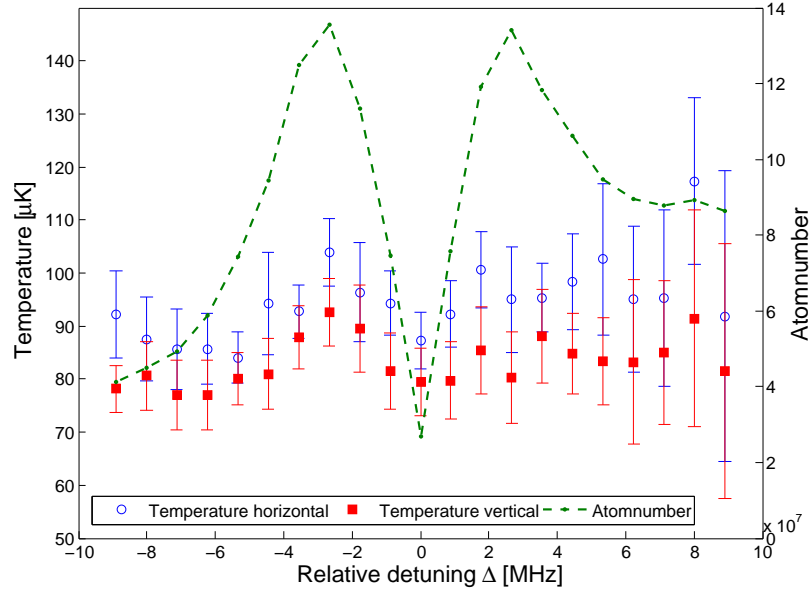


Figure 4.9.: Temperature of the atom cloud depending on the relative detuning Δ . Also shown is the atom number.

The blue circles denote the temperature in the horizontal axis, the red squares the temperature in the vertical axis and the green connected dots depict the number of atoms. Three experimental runs were performed and the error bars stem from the fit of the temperature. For this measurement we extended the time of the single-colour MOT at the end of the loading to 20 ms. Loading time was kept at 15 s. The relative detuning Δ was scanned from +8.9 MHz to -8.9 MHz in 21 steps (0.9 MHz step size) In order to measure the temperature images were taken after times of flight of 10, 12, 14, 16, 18 and 20 ms so we can get good fits for the temperature of the cloud (details to fitting can be found in the theory section 2.10).

This procedure gets the temperature of the atom cloud as low as 100 μK . The measurements show that we can get the same temperatures for the dual-colour MOT where we have higher atom numbers compared to the single-colour MOT.

Measurement in both directions should deliver the same temperature as a result. In this measurement the vertical temperature is always slightly lower than the horizontal one. This might be due to the fact that the MOT is slightly tilted and the fitting of the Gaussian to determine the size is not perfect.

In the papers of Sinclair et al. [20], Cao et al. [21] and Pradhan et al. [27] the temperature of the atom cloud is not considered or measured.

Fitting

In figure 4.10 depicted are two points of the above measurement. The figure on the left shows the fit for data point with the best fit at $\Delta = -3.6$ Mhz, the figure on the right shows fit for the data point with the worst fit at $\Delta = 8.9$ MHz. The time scale for the times of flight is between 10 and 20 ms and one can see that for the longer

times the size of the cloud of atoms has a bigger spread. This is because the cloud of atoms has expanded to a size larger than the imaging area for these long times.

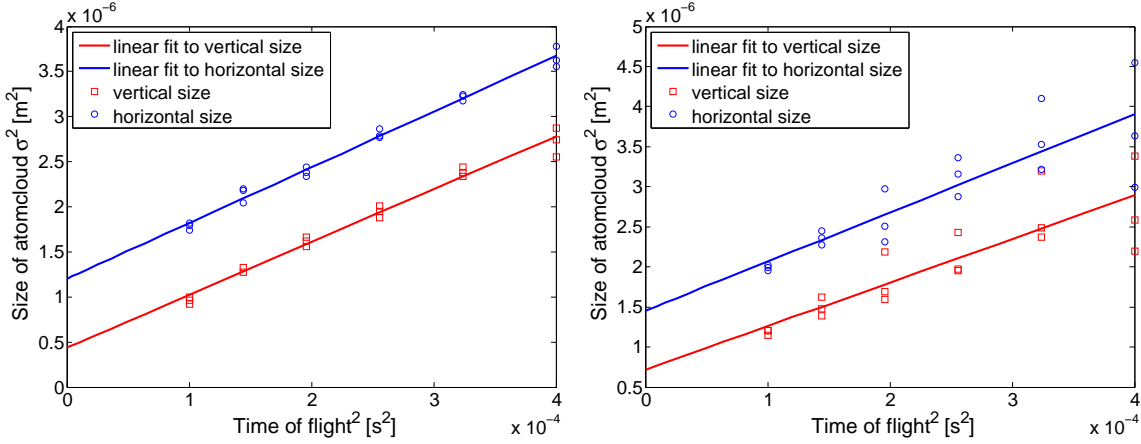


Figure 4.10.: Fits of the size of the cloud of atoms to determine the temperature. The figure of the left is for a relative detuning $\Delta = -3.6$ MHz. The right figure for a further relative detuning $\Delta = 8.9$ MHz.

4.2.9. Power

A subsequent question we were asking ourself was if the optimal relative detuning Δ changes with the total power. The idea behind this measurement is to investigate if Autler-Townes splitting has something to do with the increase in the number of atoms. The concept might be that one cooler frequency introduces a power dependent shift, which is then seen by the second frequency, resulting in a larger extension of the cloud. Since Autler-Townes splitting is dependent on the total power we should see a shift in the optimal detuning for the dual-colour MOT when we change the total power in the laser beams.

For this we attenuated the laser beams with neutral density filters. Frequency f_1 was again kept on 24.3 MHz, the loading time was 15 s and the maximum power in one beam was 34 mW. The results of the measurement are depicted in figure 4.11.

A dependence of the optimal relative detuning with the total power is not clearly shown by these measurements. Hence we don't gain valuable information from this measurement. We can not rule out that Autler-Townes splitting has an effect on the number of atoms in the dual-colour MOT. But we also do not have clear evidence that it does.

The imbalance in the figure might be due to the fact that the optimal base frequency f_1 for the MOT changes with the total power.

The papers mentioned in the introduction contain no experiments investigating the total power.

4.3. Conclusion

We have shown that we can achieve higher numbers of atoms with the dual-colour MOT than with a single-colour MOT. The reason for the higher number of atoms

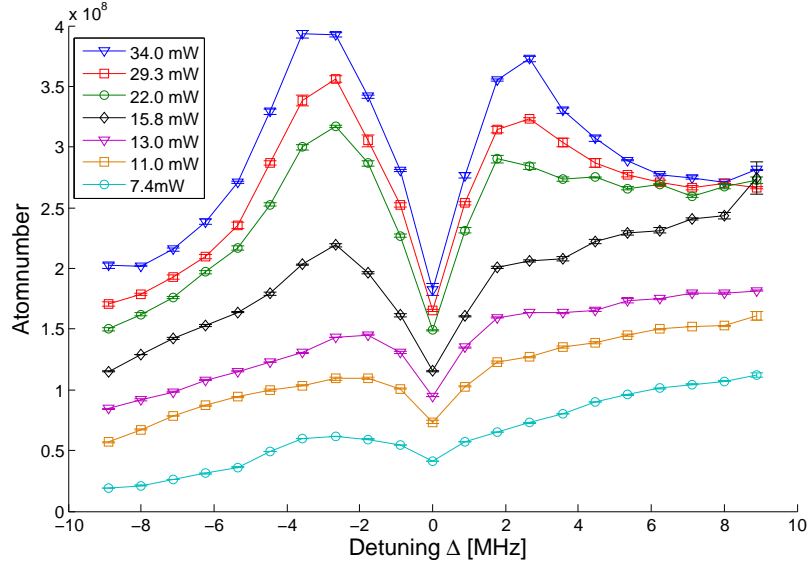


Figure 4.11.: Atom numbers depending on the total laser power and the relative detuning Δ .

can be explained by lower losses due to a lower density of the cloud of atoms (see also section 2.9). The lower density of the atom cloud is explained by an increase in volume. Investigations if Autler-Townes splitting is responsible for this increase in volume did not deliver clear results.

We could transfer the MOT into a Gaussian shape to be able to get good fits for temperature and so we will be able to load it into a magnetic trap efficiently. After 10 s of loading the number of atoms of the dual-colour MOT is about twice as high as the single-colour MOT, at long times it saturates at about four times the value. Therefore we can achieve quicker loading of a specific number of atoms or get larger MOTs with a higher number of atoms after loading for longer times. Further we are able to cool these atom clouds to the same temperature for single- and dual-colour MOTs ($\approx 100 \mu\text{K}$). What we don't understand yet is the splitting of the MOT in the dual-colour case and what might be causing this effect. Further investigations into this matter are currently conducted.

5. Towards ultra-close trapping

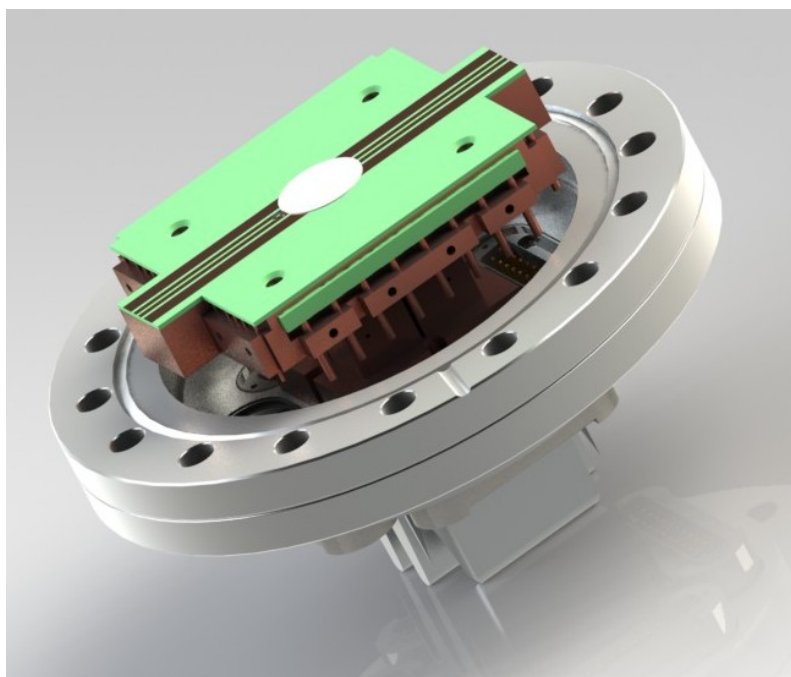


Figure 5.1.: A rendered image of the mounting

5.1. Introduction

This chapter describes our plans to bring cold atoms very close to surfaces (below $1\text{ }\mu\text{m}$) and the design of a mounting for these future experiments. Atoms trapped very close to a surface will interact with objects on the surface. For example, it is possible to couple a cold cloud of atoms to a superconducting qubit if one can get the cloud close enough to the qubit [28]. The closer the cloud of atoms is to the qubit, the stronger the interaction will be. If a good enough performance is achieved this system represents a quantum memory. A problem for trapping atoms very close to a surface is the Casimir-Polder force [29]. This attractive force pulls the atoms towards the surface, they escape from the trap and are lost for the experiment. A way to reduce the Casimir-Polder force is to make the surface as thin as possible. Our experiments will use thin membranes (a few tenth of nm thick) to probe the Casimir-Polder force and to show ultra-close trapping at these membranes or graphene.

The whole design and construction of the mounting has been done in a specialised CAD software.¹ The mounting will hold the components of the experiment like

¹SolidWorks v12.1, Dassault Systèmes (www.solidworks.com).

the thin membranes and an atomchip and includes electric feedthroughs to provide currents for diverse applications.

5.2. Five-beam MOT

For our future experimental set-up we need a MOT close to a chip or printed circuit board (PCB) that generates a magnetic trap to which we can transfer the atom cloud. This surface limits the optical access and makes a six-beam MOT very hard to realise. Many experiments, for example [30] or [31] solve this issue by using a 45°-reflection MOT² (see also Figure 5.2).

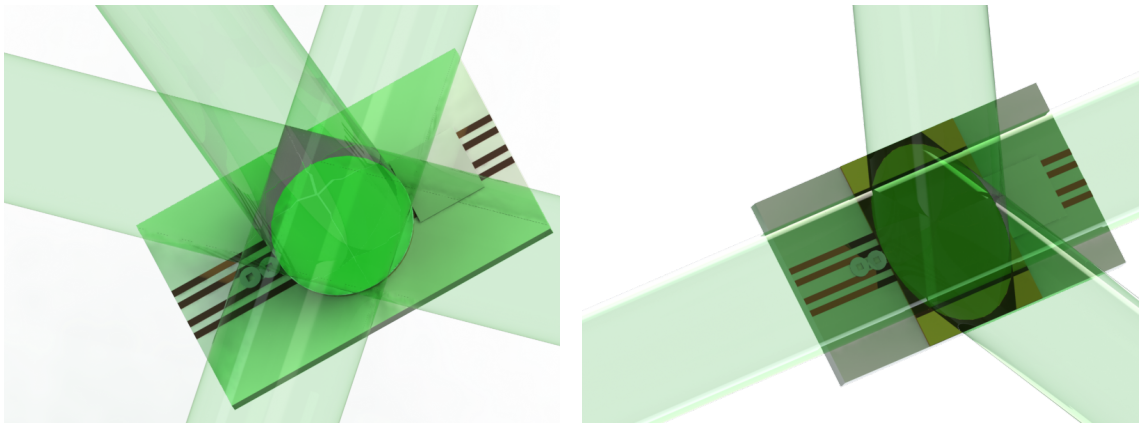


Figure 5.2.: Laser beam set-up and chip surface for five-beam MOT (left) and 45°-reflection MOT (right).

Since our samples and sample holders are non-reflective this 45°-reflection MOT can not be at the position of our samples and we need a transport system to move the cold atoms from the MOT region to the samples. Because we will need a transport system anyway we choose to use a five-beam MOT because it has other advantages over the 45°-reflection MOT (see below). This MOT is formed by two pairs of counter propagating horizontal beams and one vertical beam which is counter-reflected into itself by a reflection coated $\lambda/4$ -plate on the top surface (see also Figure 5.2). The $\lambda/4$ -plate is needed for the reflected beam to have the correct polarisation.

The main advantage of the five-beam MOT over the 45°-reflection MOT is the needed magnetic quadrupole field. In the 45°-reflection MOT case a 45°-tilted quadrupole field is necessary. This can either be provided by tilted anti-Helmholtz coils³ that obstruct the optical access or by well designed electric structures beneath the surface in combination with a magnetic bias field [31]. The five-beam MOT needs a normal quadrupole field that can be generated by anti-Helmholtz coils that do not obstruct the optical access like seen in our set-up in section 3.2.2 in figure 3.7.

²45°-reflection MOT: two counter propagating beams are reflected on the mirroring surface of the atomchip. The reflections of the beams work as additional beams. In the overlapping region of these four beams two additional orthogonal beams form the MOT.

³Anti-Helmholtz coil: Two coils in Helmholtz configuration but with one current inverted. The result is not a homogeneous field but a quadrupole field.

5.3. Magnetic fields

This section covers simulations on the trapping fields of the transport system and the MOT fields. They have been made to get approximate values for current and number of layers for the design of the multi-layer printed circuit boards (PCBs). The idea behind using multi layered PCBs is to be able to recycle current. Looping current and letting it flow in the same pattern in additional layers generates strong magnetic fields with low current values. Since the generated heat goes with the square of the current, a low current ensures that the mounting does not heat up too much (see section 5.4.3 on temperature simulations). More detailed descriptions of the PCBs are in section 5.4.2. For these quick simulations the software Mathematica⁴ was used.

Two different simulations have been carried out, one for the MOT coil PCB that generates the quadrupole field for the MOT and a second one for the magnetic trapping field produced by the transport PCB. The simulations use the Biot-Savart law which denotes the magnetic field generated by a current in an infinitely thin wire

$$\vec{B} = \frac{\mu_0}{4\pi} \int_C \frac{I d\vec{l} \times \vec{r}}{|\vec{r}|^3}, \quad (5.1)$$

where $\mu_0 = 4\pi \cdot 10^{-7} \frac{\text{Vs}}{\text{Am}}$ is the vacuum permeability, I is the current in the wire, $d\vec{l}$ is the differential vector element of the wire and \vec{r} is the displacement vector.

5.3.1. Magnetic trapping structures

For the transport system we will be using a similar concept as the transport system of Long et al. [30]. It is a magnetic conveyor belt generated by electric currents through conductive paths in a layered PCB. Three longitudinal conductive paths are used to generate a magnetic field minimum along the transport direction which confines the atoms in the radial direction. Different currents in six horizontal meandering conductive paths generate a periodic field that confines the atoms in the longitudinal direction. By changing these currents the trap minimum can be moved along the longitudinal direction and with it the atoms.

The difference in our system is that we will be using four conductive paths for the longitudinal trapping field instead of three conductive paths used by Long et al. Also these paths will not be single paths but a stack of paths in different layers, so we can recycle the currents and therefore have lower values for the currents. Additional to transport this set-up will allow us to position the cloud of atoms precisely and change the size and shape of the trap. The simulation is for the radial confinement and considers only the longitudinal trapping paths. The longitudinal confinement in the transport direction is generated by the transport wires and not considered in this simulations.

The magnetic trapping structures consist of four parallel conductive paths in multiple layers. By approximating a wire as infinitely long and thin the equation (5.1) simplifies to [32]

$$\vec{B}(x, y) = \frac{\mu_0 \cdot I}{2\pi r} \vec{e}_\phi, \quad (5.2)$$

⁴Mathematica, Wolfram Research Co. (www.wolfram.com).

where $r = \sqrt{x^2 + y^2}$ is the displacement vector. Because of the infinitely long wire one dimension is extinguished and we obtain a two-dimensional solution.

By adding up the B-fields of all the wires we get an approximation of the total B-field above the transport PCB which can be seen in figure 5.3.

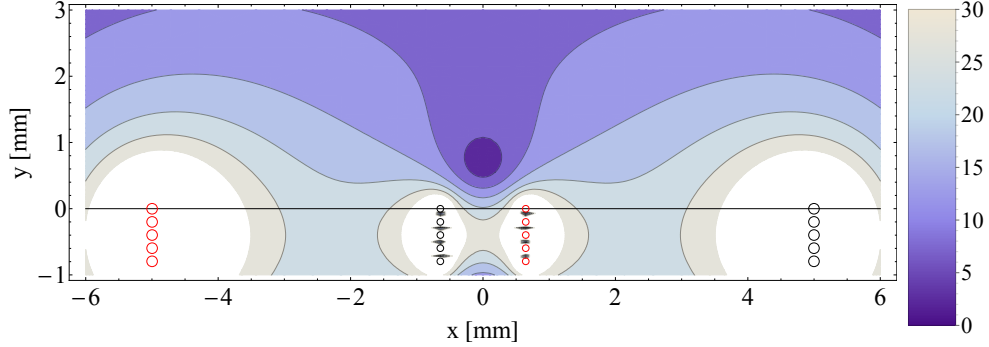


Figure 5.3.: Simulation of magnetic flux density of the trapping field generated by the transport PCB. The line at zero denotes the surface of the PCB. Plotted is the absolute value of the total magnetic field. The unit of the legend is Gauss.

The two inner stacks of conductive paths carry the same current but in opposite directions (small circles in figure 5.3). The same applies to the two outer stacks of current carrying conductive paths (large circles in figure 5.3). The colour of the circles denotes the direction of the current.

The distance between layers is 200 μm . The optimisation has been performed for the trap centre being separated 700 μm from the top layer. Six layers emerged to be a good value and the optimisation delivers values for the distances of the conducting paths and the current ratio between inner and outer conducting paths. More layers would reduce the currents in all layers but each added layer is further from the trap and contributes less to the total field. Furthermore each added layer adds to the total resistivity and makes the PCB thicker and more difficult to fabricate. The optimal distance between the inner paths is 1.3 mm the distance for the outer paths 10 mm. With these distances the currents for a field gradient of 100 G/cm at the trap minimum yields 1.6 A in the inner conductive paths and 3.7 A in the outer paths. These currents are low enough to prevent overheating of the set-up (see section 5.4.3 on temperature simulations).

5.3.2. MOT coils

The magnetic quadrupole field for the MOT could be provided by external anti-Helmholtz coils (see also section 2.4). We want to go a different route for our experiment. A multi-layer PCB with concentric conductive paths that form concentric coils will be used to generate the quadrupole field. The same concept although with less layers has been employed by Piccardo-Selg [33] for the iSense project.⁵ It has the advantage of being integrated therefore small and light. Since these coils on the PCB are much closer to the MOT area than external coils lower currents are needed to form the necessary B-field gradients. This fact plus the fact that

⁵iSense project (www.isense-gravimeter.eu).

these fairly low currents can be easily controlled made us feel confident about this approach.

Two concentric coils in the same plane will generate two quadrupole fields out of the plane (one at the front, one in the back) if the currents in the coils have an appropriate ratio and different directions. Our design uses three concentric coils. The outer and middle coil are used for the MOT. By increasing the current in the inner coil and decreasing the current in the middle coil we can move the MOT closer to the surface and transform it into a compressed MOT.

A typical quadrupole field for a MOT has a gradient of ≈ 10 G/cm along the strong axis. The goal of the optimisation was to achieve this with low current values.

The conductive paths in the MOT coil PCB are approximated by concentric loops in multiple layers. The generated B-field has cylindrical symmetry. We are most interested in the B-field on the axis of these loops because at the area where the B-field becomes zero it resembles in good approximation a quadrupole field. For this special case equation (5.1) can be simplified to [32]

$$B_z(x = y = 0, z) = \frac{\mu_0 \cdot I \cdot R^2}{2(R^2 + z^2)^{3/2}}, \quad (5.3)$$

where R is the radius of the loop.

By adding up the B-fields from all the loops we get an approximation for the B-field along the z-axis as can be seen in figure 5.4.

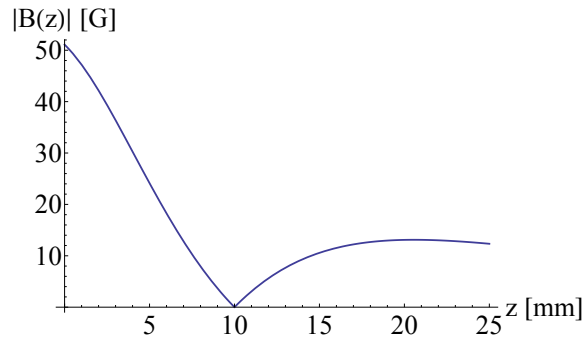


Figure 5.4.: Simulation of magnetic flux density generated by the MOT-coil PCB. Plotted is the absolute of the B-field on the z-axis normal to the surface of the PCB. The ordinate coincides with surface of the PCB.

The distance between layers is again $200 \mu\text{m}$. The optimisation has been performed for the MOT 10 mm away from the top layer for the middle and outer coils and a second time for the compressed MOT 3.2 mm away for the inner and outer coils. Twenty layers turned out to be good and the optimisation delivers values for the radii of the conducting paths and the current ratios between inner, middle and outer conducting paths. The optimal radius for the outer coil is 30 mm, for the middle coil it is 12.2 mm and for the inner one 3.7 mm. With these radii a B-field gradient of 13 G/cm at the MOT area is achieved by currents of 11.4 A in the outer conductive paths and 10 A in the middle paths. A gradient of 58 G/cm for the compressed MOT can be achieved by currents of 7.8 A in the outer coil and 4 A in the inner coil. These currents are also low enough to prevent overheating of the set-up (see section 5.4.3 on temperature simulations).

5.4. Mounting

The mounting will be an essential part of the vacuum system. Situated at the top of the experiment chamber it holds the parts for the experiments that need to be inside the vacuum. Additionally it contains electrical feedthroughs to provide currents to the experiments.

5.4.1. Prerequisites for the mounting

For the design of the mounting we have to take a lot of prerequisites into consideration. The most important ones are

- Ultra high vacuum⁶ (UHV) compatibility. Since our experiments will be running at pressures down to 10^{-11} mbar all components of the mounting need to have low outgassing coefficients and have to withstand a bakeout.⁷
- Non ferrous materials: Since the experiments need very precise control over magnetic fields to position atoms close to a surface, magnetic materials need to be avoided.
- Electric feedthroughs: the wire structures that generate the magnetic fields for the experiments need currents which are generated outside the vacuum. The needs for our experiment are: six feedthroughs with ≈ 10 A for the MOT fields and 44+ feedthroughs with up to 5 A for magnetic trapping, transport and the atomchip.
- Heat conductivity: the heat produced by the currents needs to be transported out of the chamber.
- Size restrictions by the chamber, the inner diameter of the chamber is 108 mm.
- Size restrictions by the optical access for lasers and imaging, the surface of the mounting should not protrude further than 20 mm from the top of the experiment chamber.
- No air pockets.
- Prize considerations, the system has to be feasible.

5.4.2. Design

The mounting consists of the following parts

- Transport PCB which has the conducting track structures to generate the fields for magnetic trapping to which also these components are mounted
 - Reflection coated $\lambda/4$ -plate which is used to reflect the fifth MOT-beam.

⁶Ultra high vacuum (UHV): denotes a vacuum of pressures lower than 10^{-9} mbar.

⁷Bakeout: to achieve a very good vacuum it is customary to heat the vacuum chamber to 100°C-200°C while pumping down to get rid of adsorbed materials (mostly water) fast. Outgassing of the components diminishes over time and by heating them this time can be accelerated and hence lower outgassing is present after the bakeout.

- Atomchip that will form the final magnetic trap.
- Samples.
- Copper sheet to conduct and spread heat from the transport PCB.
- Copper block as a central piece to which most of the other components are attached.
- PCB for the MOT-coil conducting track structures.
- Clamps to fix the connector wires and establish a thermal contact with them.
- Copper holder to connect copper block and flange.
- Flange with electric feedthroughs.

A not to scale schematic of a cut through the mounting can be seen in figure 5.5. Visible on top is the MOT region. The MOT is turned into a compressed MOT and then loaded into the magnetic trap during the experiment cycle. The magnetic trap is also the transport system and moves the cold atoms sideways to the atomchip or the samples. In the experiment the mounting will be attached upside down so the atoms fall away from it when the traps are turned off for imaging.

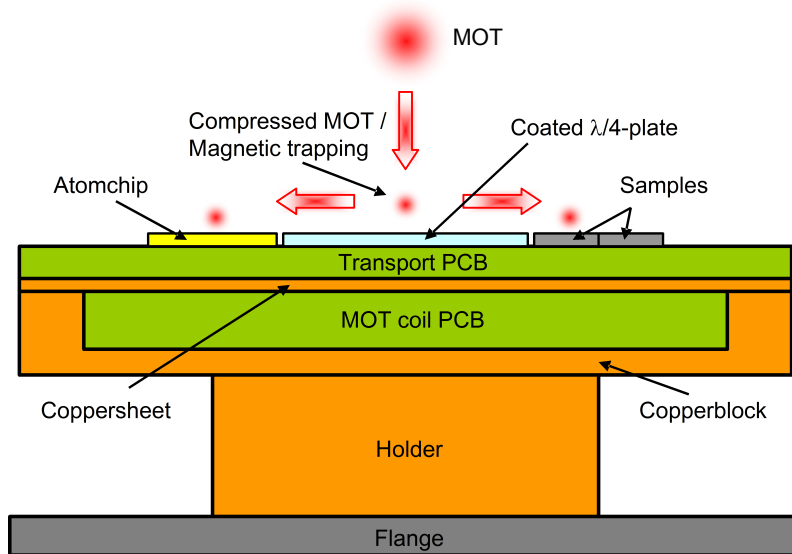


Figure 5.5.: Schematic drawing of a cut through the mounting.

Transport PCB

The PCB is made out of a special material⁸ which has low outgassing coefficients and is therefore viable in UHV. The drawback of this material is its low thermal conductivity of only $\approx 0.7 \frac{\text{W}}{\text{mK}}$ [34].

The magnetic fields generated by the transport PCB are used to magnetically trap the atoms and transport them from the MOT region to the atomchip or the samples (details in section 5.3.1).

⁸RO4350B, Rogers corp. (www.rogerscorp.com).

On three sides of the rim of the bottom of the transport PCB are solder pads to connect the wires from the feedthroughs. A few of these pads are connected to pads at the top of the PCB where an atomchip might be mounted and connected via wire bonding. Solder connections in UHV applications, albeit uncommon, are possible with a special solder. If this approach fails to deliver the desired results, glueing of the connections with a special glue would be an alternative as used in the work of Piccardo-Selg [33].

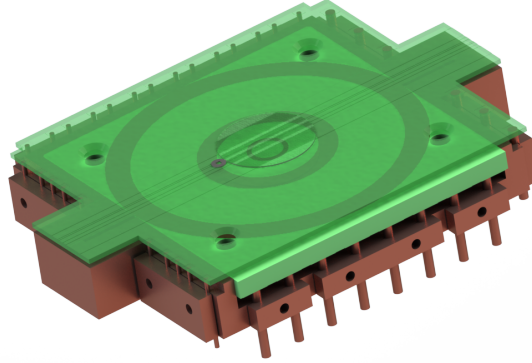


Figure 5.6.: PCBs, clamps and copper block. The transport PCB is see-through, the copper sheet is not visible.

On top of the PCB, in the middle, the reflection coated $\lambda/4$ -plate is positioned. Next to it are the samples/sample holders. The final object that may be on top of the transport PCB next to the reflection coated $\lambda/4$ -plate is an atomchip.

Copper sheet

The copper sheet is 1 mm thick, has almost the same size as the transport PCB and is located directly below it. Its main purpose is to conduct and spread the generated heat. 1 mm thickness is enough to transmit the heat from the transport PCB to the copper block efficiently. This has been determined by temperature simulations (see section 5.4.3). Another concern is the distance of the MOT-coil PCB. By making the copper sheet thicker the MOT-coil PCB would be further away from the MOT region and would need higher currents to provide the necessary B-field gradients at the same position (see section 5.3.1). Like all the other copper components the copper sheet is made out of oxygen-free copper (OFC). This was chosen because normal copper is detrimental for UHV applications because of outgassing. Copper was chosen for its excellent heat conductivity and because it is non-magnetic.

Copper block

The copper block is the centre-piece of the mounting. It sits right below the copper sheet and conducts heat further. It has a slot that holds the MOT-coil PCB. Grooves on the side accommodate the wires which are pressed there by clamps. Tap holes between the grooves take in the screws that fix the clamps.

All the tap holes have ventilation holes from the bottom to prevent air pockets. With four holes at the bottom the copper block can be mounted to the copper holder.

Slits through the material will reduce Eddy-currents that arise when switching the currents for the magnetic fields.

MOT-coil PCB

The transport PCB is another multi layer PCB that is used to generate the magnetic fields for the MOT (see section 5.3.2). One the rim of one side of the bottom are solder pads to connect the wires that provide the currents. Where necessary, Kapton foil will provide electrical isolation.

Clamps

The clamps are mounted with screws to the side of the copper block. Their function is to establish a thermal contact between the electrically insulated wires and the copper block and to fix the wires in place at the same time. The grooves in the sides of the clamps that accept the wires are slightly shallower than the ones on the copper block. This ensures that the clamps do not touch the copper block and the wires are thoroughly pressed against it. A render of this aspect of the design is depicted in figure 5.7.

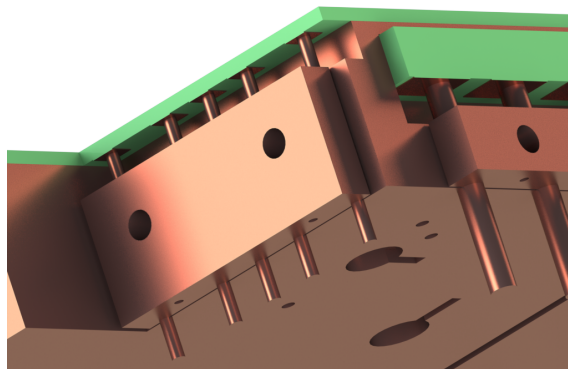


Figure 5.7.: Closeup of solderpads and clamps. Not visible are the screws that fix the clamps.

Copper holder

The copper holder connects the copper block and the flange and ensures a good thermal conductivity to transport heat to the outside. It also functions as a spacer and its height defines the final position of the experiment in the chamber. Four tap holes at the top provide a way to mount the copper block. Holes on the sides cater for the ventilation of these tap holes.

Through pockets on the sides of the bottom the copper holder is mounted to the flange. Slits through the centre help reduce Eddy currents.

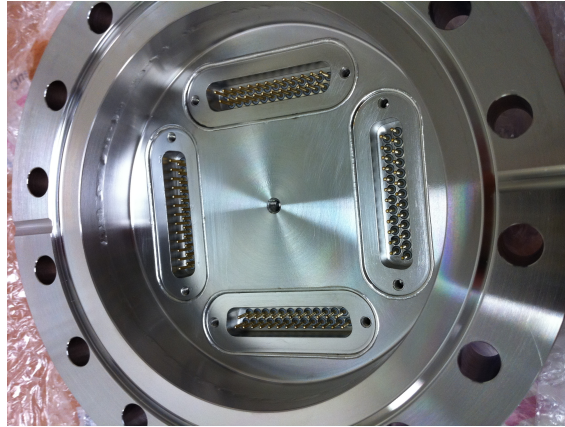


Figure 5.8.: Photo of the inside of the custom made flange.

Flange

The flange was custom made by the company LewVac and has four 25-pin sub-D electric feedthroughs.⁹ In the middle of the flange the copper holder is mounted. Ventilated screws have to be used because the tap holes of the flange are not vented. The feedthroughs are arranged in a square around the holder. Each pin of the feedthroughs can accept a current of 5 A. The higher currents for the MOT coils (≈ 10 A) will be using multiple pins to spread the load. Not all of the 100 available pins are used but it's always smart to have a few extra to be flexible for future experiments.

There is a recess in the flange to ensure enough space for the mounting so that it does not protrude too much into the chamber and blocks optical access and the MOT laser beams. The connector of the flange is a ConFlat DN100 and will be attached top down to the top of our chamber. A picture of the flange can be seen in figure 5.8.

On the vacuum side the wires are connected to the feedthroughs by crimp pins. Tap holes on the air side provide means to mount a heatsink.

5.4.3. Temperature simulations

One of the big questions during the design process was how much heat would be generated by the currents. Will the temperature get too high and have detrimental effects on the mounting like solder connections coming undone or deformations of the parts? To lessen this concern, temperature simulations with SolidWorks were carried out. Since this software was not predominantly designed for temperature simulations it is not the best in this respect. The simulation data still gives us a good clue about what temperatures we will have to expect.

The first step in creating a temperature simulation is applying material properties to the components and creating a mesh. Next is, to assign heat sources and cooling mechanisms. In our case the heat sources are the current carrying PCB structures and the solder pads. The only cooling mechanism we took into consideration is thermal convection of air at room temperature on the air side of the mounting.

⁹W-SUBD-25-DE-CE-SSG, VACOM Vakuum Komponenten & Messtechnik GmbH (www.vacom.de).

With a total of ≈ 25 W of heat power distributed realistically over the PCB structures and solder pads we get acceptable results as can be seen in figure 5.9. This is a steady state simulation that uses mean values for the heat powers and gives a steady state temperature distribution for the whole mounting.

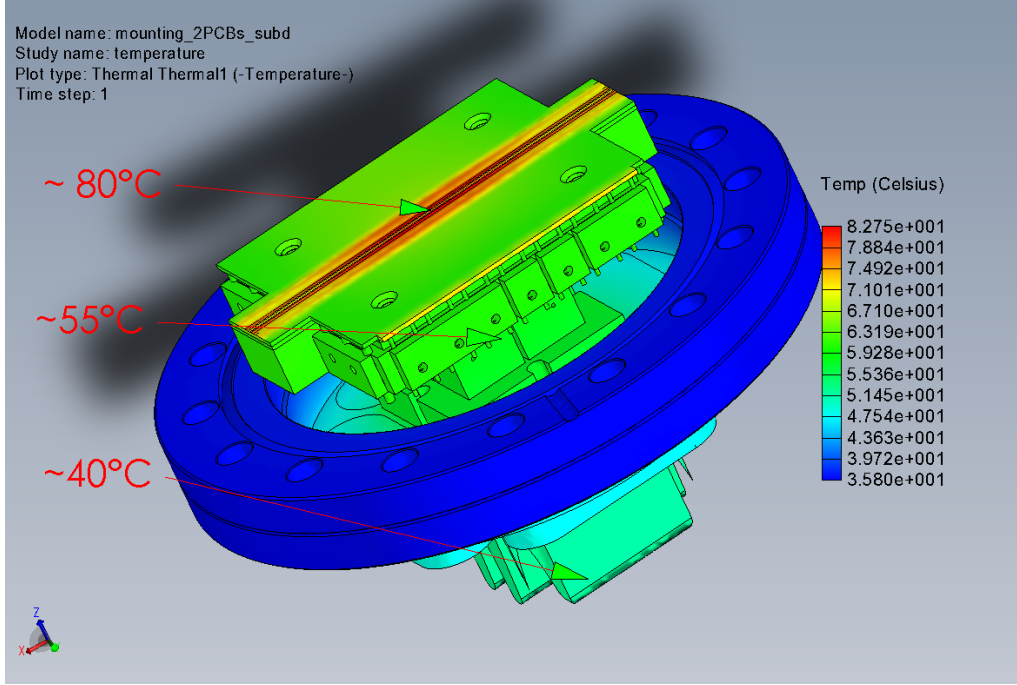


Figure 5.9.: Temperature simulation of the mounting.

The real experiment cycle will not have the currents for trapping and the currents for the MOT-coils on at the same time. At the start of the cycle the currents for the MOT-coils are on. After loading the MOT the currents for trapping are switched on, the atoms are transferred to the magnetic trap and the currents in the MOT-coils are switched off. At the end of each experiment cycle all the currents are off for a short downtime. For the simulation we assumed a duty cycle of 50/50 between currents of the two PCBs.

To determine the generated heat $P = U \cdot I = I^2 \cdot R$ we need the current in the wires I and the resistance of the PCB structure and the solder pads R . The resistance of the PCB structures can be calculated by

$$R_{PCB} = \frac{\rho_{copper} \cdot l}{A} \quad (5.4)$$

where l is the length and A is the area of the cross section of the conductor. Typical PCBs have a thickness of the copper layer of $70 \mu\text{m}$, hence the area A is $70 \mu\text{m}$ times the width of the conducting path. The resistance of the MOT-coils is $\approx 100 \text{ m}\Omega$, the resistance of the trapping conducting paths are $\approx 240 \text{ m}\Omega$. The contact resistance of the solder pads has been measured and is $\approx 28 \text{ m}\Omega$.

With currents of 10 A in the MOT-coils we get 10 W of heat power in both coils and additionally 4×1.6 W on four solderpads of the MOT-coil PCB. The currents in the trapping structure are ≈ 3 A and generate heat of 6 W in each of the outer conducting paths and 5 W in each of the inner conducting paths. In addition 2 W are distributed over 14 contacts on the transport PCB. Due to the duty cycle of 50/50

the average values for the simulation are half of these values. The total average of these heat powers is ≈ 25 W. The current values were deduced from the magnetic field simulations in section 5.3.

This simulation is only one example of the final design. More simulations have been made during the design process to determine how high the currents in the PCB structures can be and how we have to dimension the parts. Especially the thickness of the copper sheet was crucial. If it is too thin the transport PCB will heat up too much, if it is too thick the MOT-coil PCB will be further from the MOT region and will need higher currents to provide the necessary magnetic field gradients. The simulations have shown that 1 mm thickness of the copper sheet is enough to spread and transport the heat from the transport PCB efficiently.

Since the simulations on magnetic fields and this thermal simulation are intertwined by the current values and dimensions of the parts, some iterations between the simulations had to be performed.

This simulations point out a distinct advantage of the approach of using PCBs for the magnetic fields and recycling the currents. The fairly low heat power generated can be transported by heat conductance of copper parts to the outside of the chamber and no additional cooling is required. In addition the low values for the currents makes it easier to control them precisely. For comparison in the paper of Wildermuth et al. [31] they use a U-shaped copper understructure with a typical current of 60 A to generate the B-fields for the MOT.

6. Conclusion and outlook

Within the framework of this thesis a novel set-up for a magneto optical trap has been investigated. The experimental set-up has been developed further to achieve this and the laser set-up has been adapted and perfected. The vacuum chamber was prepared and brought to the low pressures required. An imaging system has been designed and set up. The experimental control was installed and connected to the experiment. Finally measurements on a dual-colour magneto-optical trap were conducted and the resulting data was analysed and evaluated. Additionally a mounting for future experiments was designed. During this process, simulations on thermal properties and magnetic fields were conducted.

The investigation of the dual-colour MOT was a partial success. We did manage to get four times the number of atoms in the same loading time than a single-colour MOT with the same laser power. We further managed to get the cloud of atoms, which was deformed because of the dual-colour set-up into a Gaussian shape to be able to perform thermometry. Furthermore we achieved cooling them to low temperatures (100 μ K) so loading to a magnetic trap should be possible. What we do not understand yet, is why we have these high atom numbers and why the MOT gets deformed. Experiments investigating this matter have not given conclusive evidence to support our theories.

The design of a mounting for future experiments on ultra-close trapping was conducted. Numerous aspects and factors were taken into consideration for this design. Simulations of magnetic fields were undertaken to obtain approximate values for the dimensions of the current carrying structures and the expected currents. With these values we conducted thermal simulations on the temperature distribution of the mounting during operation. Because of these simulations we were able to design the mounting with the confidence that it will be satisfactory for the future experiments.

Further experiments on the dual-colour MOT will be performed to fathom the reasons for the peculiar shape of the MOT and physical effects that lead to them. This could turn out to be very interesting because simple theories we made were disproved by the experimental results. After we figure out the exact mechanics behind the dual-colour MOT we might even be able to further optimise the MOT.

After the mounting has been built it will be put into the set-up and experiments on ultra-close trapping will commence. The first step will be to create the dual-colour MOT with the five-beam set-up and the magnetic fields from the current structures of the mounting. Next will be compressing the MOT and loading it into the magnetic trap of the transport current structures. After that transport and positioning of the atom cloud will be investigated. Therefore an additional imaging system will be implemented to be able to image the atom cloud with high resolution from two different sides. After transporting the cloud of atoms, measurements on

ultra-close trapping can be done by placing the atom cloud very close precisely over thin membranes. A different way to investigate ultra-close trapping will be to load the atom cloud from the magnetic transport trap to a chip trap on an atomchip. The trapping structures on the atomchip will be able to confine the atoms even stronger and therefore will also enable us to achieve a BEC by evaporative cooling. This BEC could be used to investigate ultra-close trapping with a thin free-standing membrane on the atomchip.

A. Technical drawings

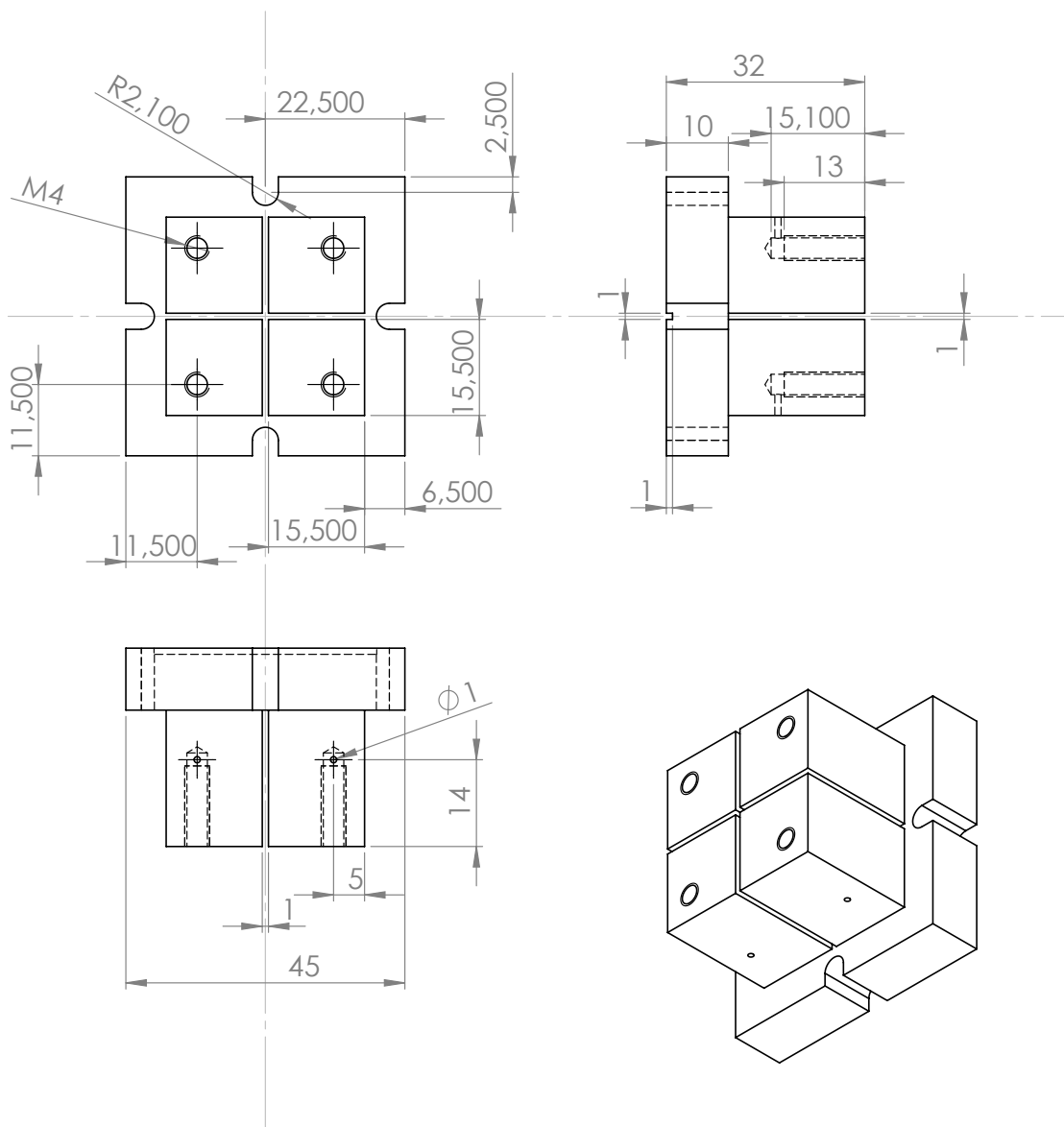


Figure A.1.: Technical drawing of the copper holder.

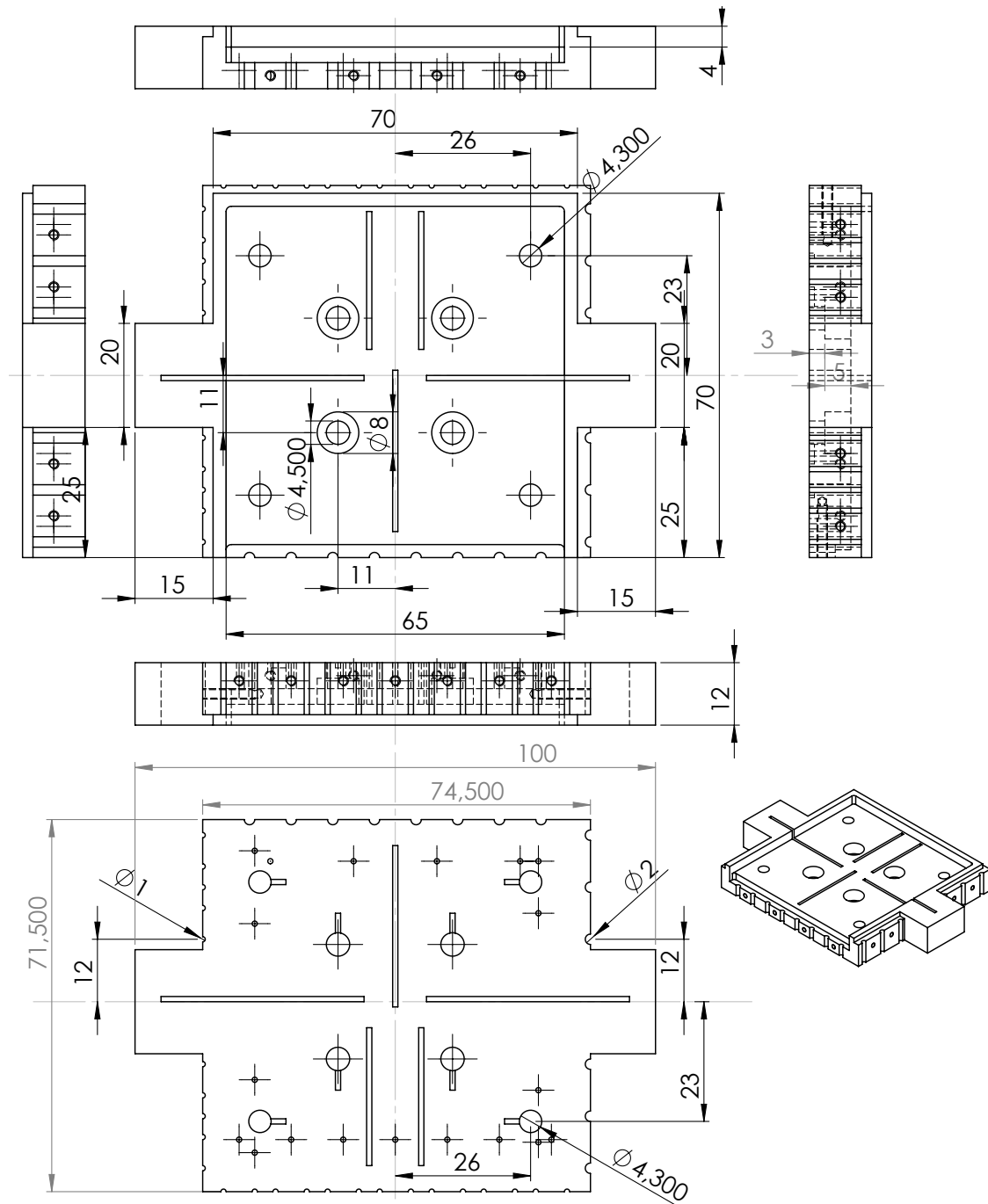


Figure A.2.: Technical drawing of the central piece, the copper block (Sheet 1 of 3).

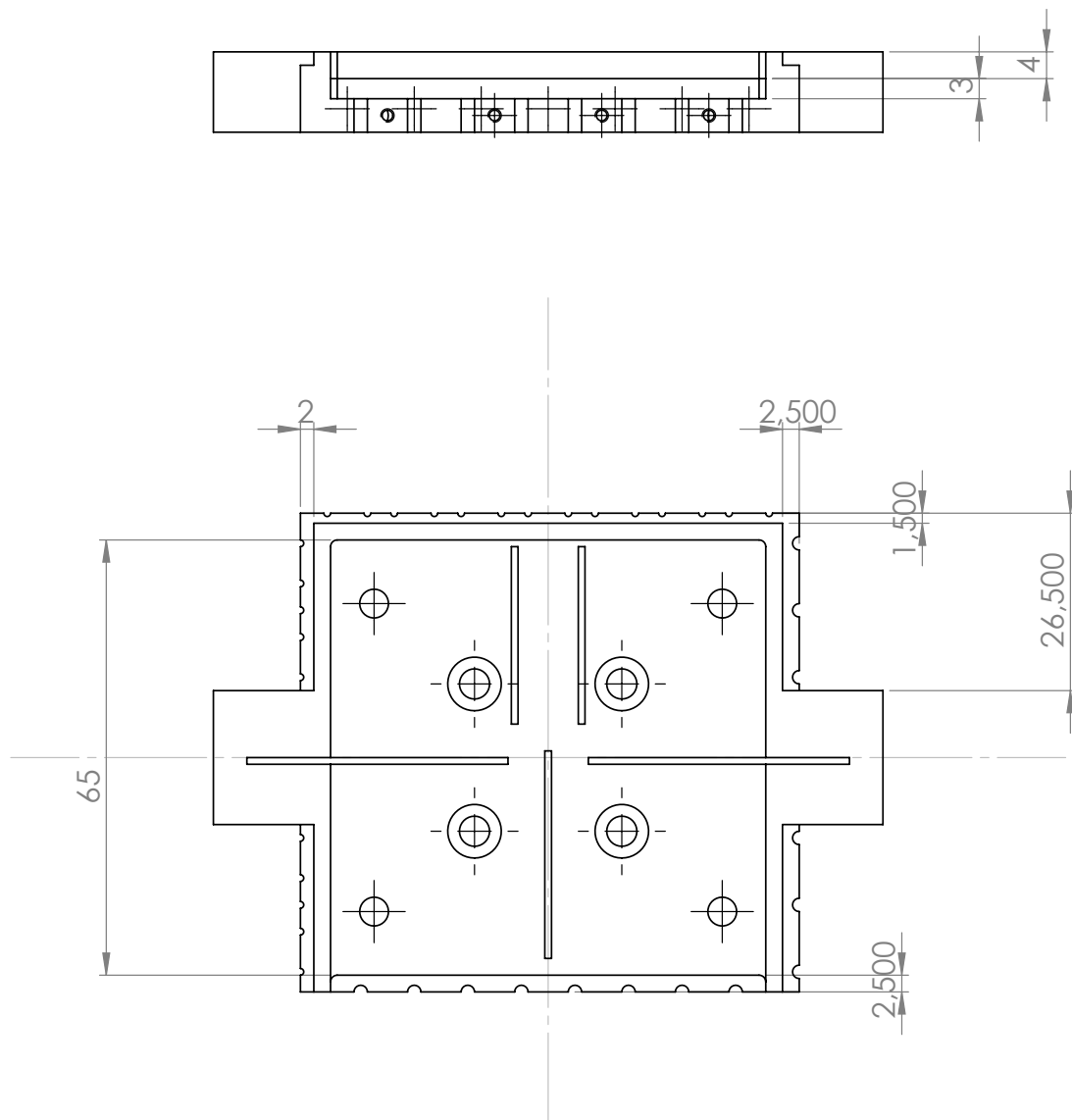


Figure A.3.: Technical drawing of the central piece, the copper block (Sheet 2 of 3).

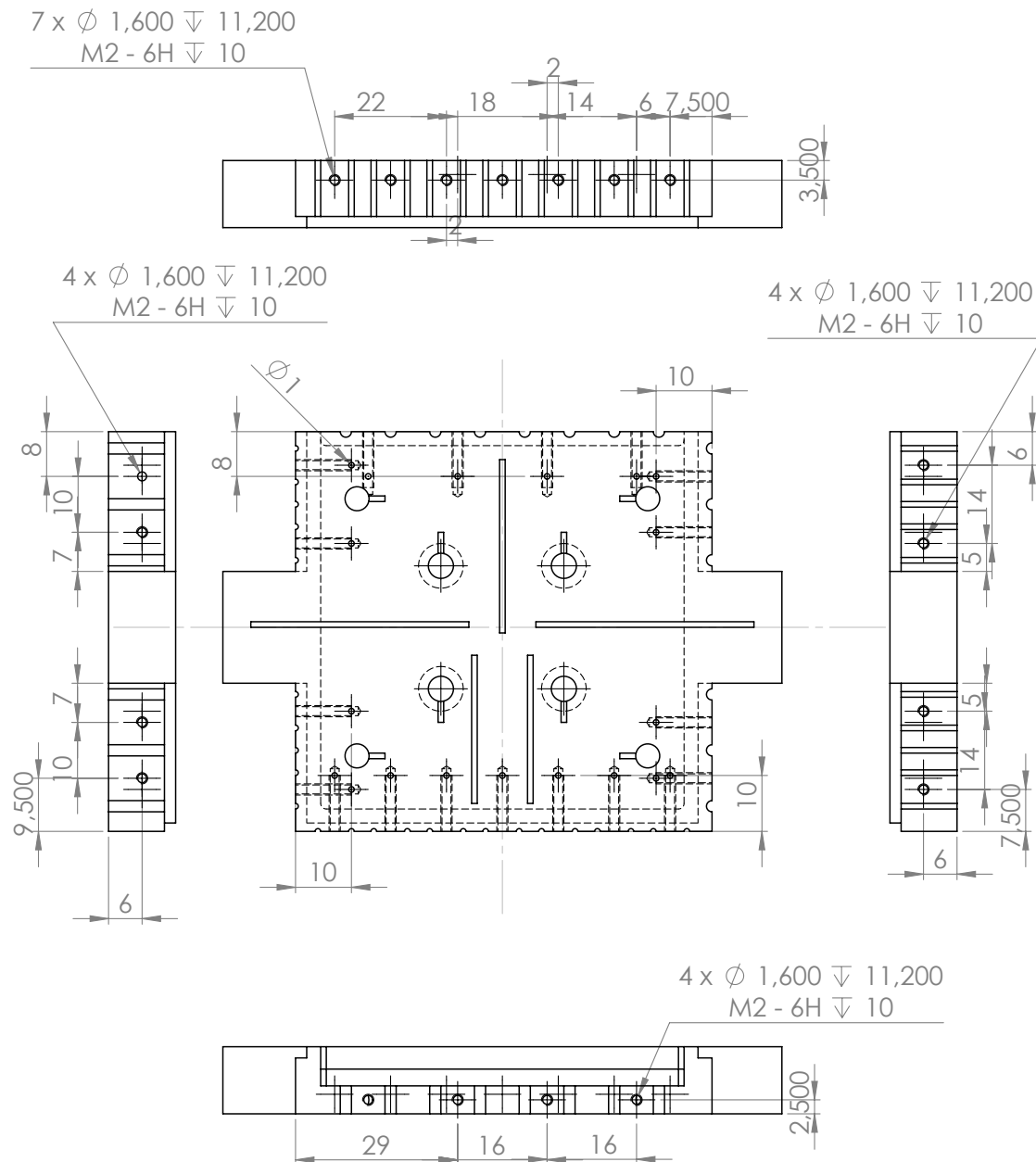


Figure A.4.: Technical drawing of the central piece, the copper block (Sheet 3 of 3).

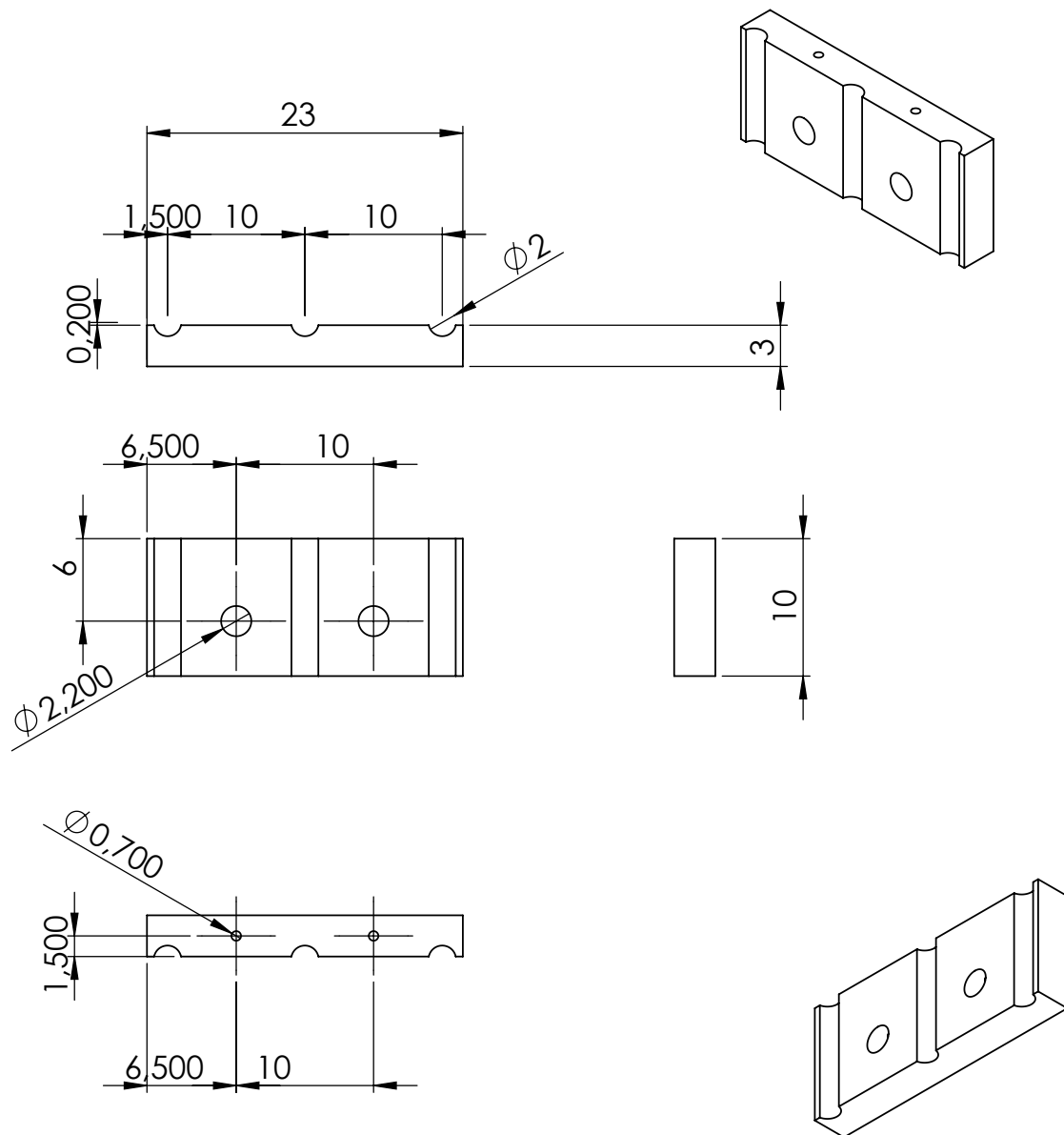


Figure A.5.: Technical drawing of a clamp which fastens the wires to the copper block.

Bibliography

- [1] Steven Chu. The manipulation of neutral particles. *Reviews of Modern Physics*, 70(3):685–706, 1998. 6
- [2] C Cohen-Tannoudji. Manipulating atoms with photons. *Physica Scripta*, 70(3):707–719, 1998. 6
- [3] WD Phillips. Laser cooling and trapping of neutral atoms. *Reviews of Modern Physics*, 70(3):721–741, 1998. 6
- [4] K B Davis, M O Mewes, M R Andrews, N J Van Druten, D S Durfee, D M Kurn, and W Ketterle. Bose-Einstein Condensation in a Gas of Sodium Atoms. *EQEC96 1996 European Quantum Electronic Conference*, 75(22):3969–3973, 1996. 6
- [5] M H Anderson, J R Ensher, M R Matthews, C E Wieman, and E a Cornell. Observation of bose-einstein condensation in a dilute atomic vapor. *Science (New York, N.Y.)*, 269(5221):198–201, July 1995. 6
- [6] C C Bradley, C A Sackett, J J Tollett, and R G Hulet. Evidence of Bose-Einstein condensation in an atomic gas with Attractive Interactions. *Physical Review Letters*, 75(9):1687–1690, 1995. 6
- [7] EA Cornell and CE Wieman. Nobel Lecture: Bose-Einstein condensation in a dilute gas, the first 70 years and some recent experiments. *Reviews of Modern Physics*, 74(July), 2002. 6
- [8] Wolfgang Ketterle. When atoms behave as waves: Bose-Einstein condensation and the atom laser (Nobel Lecture). *Chemphyschem : a European journal of chemical physics and physical chemistry*, 3(9):737–53, September 2002. 6
- [9] Stephan Wildermuth, Sebastian Hofferberth, Igor Lesanovsky, Elmar Haller, L Mauritz Andersson, Sönke Groth, Israel Bar-Joseph, Peter Krüger, and Jörg Schmiedmayer. Bose-Einstein condensates: microscopic magnetic-field imaging. *Nature*, 435(7041):440, 2005. 6
- [10] S. Wildermuth, S. Hofferberth, I. Lesanovsky, S. Groth, P. Krüger, J. Schmiedmayer, and I. Bar-Joseph. Sensing electric and magnetic fields with Bose-Einstein condensates. *Applied Physics Letters*, 88(26):264103, 2006. 6
- [11] Immanuel Bloch, Jean Dalibard, and Sylvain Nascimbène. Quantum simulations with ultracold quantum gases. *Nature Physics*, 8(4):267–276, April 2012. 6

- [12] W S Bakr, a Peng, M E Tai, R Ma, J Simon, J I Gillen, S Fölling, L Pollet, and M Greiner. Probing the superfluid-to-Mott insulator transition at the single-atom level. *Science (New York, N.Y.)*, 329(5991):547–50, July 2010. 6
- [13] LV Hau, SE Harris, Zachary Dutton, and CH Behroozi. Light speed reduction to 17 metres per second in an ultracold atomic gas. *Nature*, 397(February):594–598, 1999. 6
- [14] Chien Liu, Zachary Dutton, CH Behroozi, and LV Hau. Observation of coherent optical information storage in an atomic medium using halted light pulses. *Nature*, 409(January), 2001. 6
- [15] T Chanelière, D N Matsukevich, S D Jenkins, S-Y Lan, T a B Kennedy, and a Kuzmich. Storage and retrieval of single photons transmitted between remote quantum memories. *Nature*, 438(7069):833–6, December 2005. 6
- [16] E. Vetsch, D. Reitz, G. Sagué, R. Schmidt, S. T. Dawkins, and a. Rauschenbeutel. Optical Interface Created by Laser-Cooled Atoms Trapped in the Evanescent Field Surrounding an Optical Nanofiber. *Physical Review Letters*, 104(20):203603, May 2010. 6
- [17] K. Dieckmann, R. Spreeuw, M. Weidemüller, and J. Walraven. Two-dimensional magneto-optical trap as a source of slow atoms. *Physical Review A*, 58(5):3891–3895, November 1998. 6
- [18] W Ketterle, Kb Davis, Ma Joffe, A Martin, and De Pritchard. High densities of cold atoms in a dark spontaneous-force optical trap. *Physical Review Letters*, 70(15):2253–2256, April 1993. 6
- [19] David Hunger, Stephan Camerer, Theodor W. Hänsch, Daniel König, Jörg P. Kotthaus, Jakob Reichel, and Philipp Treutlein. Resonant Coupling of a Bose-Einstein Condensate to a Micromechanical Oscillator. *Physical Review Letters*, 104(14):143002, April 2010. 7
- [20] AG Sinclair, Erling Riis, and MJ Snadden. Improved trapping in a vapor-cell magneto-optical trap with multiple laser frequencies. *JOSA B*, 11(12):2333–2339, 1994. 7, 25, 29, 32, 34
- [21] Qiang Cao, Xin-Yu Luo, Kui-Yi Gao, Xiao-Rui Wang, Dong-Min Chen, and Ru-Quan Wang. Improved atom number with a dual color magneto—optical trap. *Chinese Physics B*, 21(4):043203, April 2012. 7, 25, 32, 34
- [22] Harold J. Metcalf and Peter Straten. *Laser Cooling and Trapping* -. Springer, Berlin, Heidelberg, 1st ed. 1999. corr. 2nd printing 2001 edition, 1999. 8, 12
- [23] P. D. Lett, W. D. Phillips, S. L. Rolston, C. E. Tanner, R. N. Watts, and C. I. Westbrook. Optical molasses. *Journal of the Optical Society of America B*, 6(11):2084, November 1989. 9
- [24] J. Dalibard and C. Cohen-Tannoudji. Laser cooling below the Doppler limit by polarization gradients: simple theoretical models. *Journal of the Optical Society of America B*, 6(11):2023, November 1989. 10, 12

- [25] Daniel Adam Steck. Rubidium 87 D Line Data. *Journal of Geophysical Research*, 2009:31, 2010. 13
- [26] C S Adams and E Riis. Laser cooling and trapping of neutral atoms. *Progress in Quantum Electronics*, 21(1):1–79, 1997. 14
- [27] S. Pradhan, SJ Gaur, KG Manohar, and BN Jagatap. Enhancement in the number of trapped atoms in a cesium magneto-optical trap by a near-resonant control laser. *Physical Review A*, 72(5):053407, November 2005. 25, 32, 34
- [28] J. Verdú, H. Zoubi, Ch. Koller, J. Majer, H. Ritsch, and J. Schmiedmayer. Strong Magnetic Coupling of an Ultracold Gas to a Superconducting Waveguide Cavity. *Physical Review Letters*, 103(4):043603, July 2009. 37
- [29] CI Sukenik, MG Boshier, D Cho, V Sandoghar, and EA Hinds. Measurement of the Casimir-Polder force. *Physical Review Letters*, 1993. 37
- [30] R. Long, T. Rom, W. Hänsel, T. W. Hänsch, and J. Reichel. Long distance magnetic conveyor for precise positioning of ultracold atoms. *The European Physical Journal D*, 35(1):125–133, June 2005. 38, 39
- [31] S. Wildermuth, P. Krüger, C. Becker, M. Brajdic, S. Haupt, A. Kasper, R. Folman, and J. Schmiedmayer. Optimized magneto-optical trap for experiments with ultracold atoms near surfaces. *Physical Review A*, 69(3):030901, March 2004. 38, 48
- [32] Wolfgang Demtröder. *Experimentalphysik 2 (3., Bearb. U. Erw. Aufl. 2004)* -. Springer DE, Berlin, 3rd edition, 2004. 39, 41
- [33] Anton Piccardo-Selg. *Cold Atom Sources for Portable Quantum Sensors*. PhD thesis, University of Nottingham, 2013. 40, 44
- [34] Rogers Corporation. RO4000 ® Series High Frequency Circuit Materials, 2013. 43

Danksagung

Danke an meine Eltern Siegfried und Hildegard, welche mich mein ganzes Leben lang unterstützt und gefördert haben, unabhängig von meinen Entscheidungen. Danke!

Weiterer Dank geht an Chrussi welchem ich zu verdanken habe, dass ich diese Arbeit in Nottingham durchführen konnte und der mich dabei begleitet hat. Ebenfalls meinen Betreuern Peter und Thorsten sowie Bo, Samanta und Tadas mit denen bei der Arbeit im Labor keine Langeweile aufkam. Auch dem Rest der Kalten Atome Sippe in Nottingham in den Labors und Theoriekammern.

Danke auch an Freunde und Familie. Speziell an Iris, Yasmeeen, Michi, René, Heidi, Simon und Johanna. Zudem auch an meine Studienkollegen Bambi, Beuty und Anna sowie die Leute der Fachschaft Physik mit welchen ich auf etliche tolle Jahre zurückblicken kann. Zuletzt noch Dank an Joachim, welcher mir Gesellschaft beim Schreiben dieser Arbeit leistete und ohne welchen sie nicht so schnell fertig geworden wäre.